Viral and cellular determinants of polarized trafficking of viral envelope proteins from insect-specific and insect-vectored viruses in insect midgut and salivary gland cells

Authors:

Jeffrey J. Hodgson[*1,2], Robin Y. Chen[*1], Gary W. Blissard[^2#], Nicolas Buchon[^1#]

* Jeffrey J. Hodgson and Robin Y. Chen contributed equally to the work.

^ Nicolas Buchon and Gary W. Blissard contributed equally as co-senior authors.

[#] Corresponding author

[1] Department of Entomology, Cornell Institute of Host Microbe Interactions and Disease, Cornell University, Ithaca, New York, USA,

[2] Boyce Thompson Institute at Cornell University, Ithaca, New York, USA

Keywords: Envelope proteins, polarized trafficking, midgut, enterocytes, salivary gland, VSV G, GP64, arbovirus, rhabdovirus, baculovirus, YxxØ

Short title: Polarized trafficking of viral envelope proteins in insect tissues

Abstract

Systemic viral infection of insects typically begins with primary infection of midgut epithelial cells (enterocytes) and subsequent transit of the progeny virus in an apical-to-basal orientation into the hemocoel. For insect-vectored viruses, an oppositely oriented process (basal-to-apical transit) occurs upon secondary infection of salivary glands, and is necessary for virus transmission to non-insect hosts. To examine this inversely oriented virus transit in these polarized tissues, we assessed

the intracellular trafficking of two model viral envelope proteins (baculovirus GP64 and vesicular stomatitis virus G) in the midgut and salivary gland cells of the model insect, *Drosophila melanogaster*. Using fly lines that inducibly express either GP64 or VSV G, we found that each protein, expressed alone, was trafficked basally in midgut enterocytes. In salivary gland cells, VSV G was trafficked apically in most but not all cells, whereas GP64 was consistently trafficked basally. We demonstrated that a YxxØ motif present in both proteins was critical for basal trafficking in midgut enterocytes, but dispensable for trafficking in salivary gland cells. Using RNAi, we found that clathrin adaptor protein complexes AP-1 and AP-3, as well as seven Rab GTPases, were involved in polarized VSV G trafficking in midgut enterocytes. Our results indicate that these viral envelope proteins encode the requisite information and require no other viral factors for appropriately polarized trafficking. In addition, they exploit tissue-specific differences in protein trafficking pathways to facilitate virus egress in the appropriate orientation for establishing systemic infections and vectoring infection to other hosts.

Importance

Viruses that use insects as hosts must navigate specific routes through different insect tissues to complete their life cycles. The routes may differ substantially depending on the life cycle of the virus. Both insect pathogenic viruses and insect vectored viruses must navigate through the polarized cells of the midgut epithelium to establish a systemic infection. In addition, insect-vectored viruses must also navigate through the polarized salivary gland epithelium for transmission. Thus, insect-vectored viruses appear to traffic in opposite directions in these two tissues. In this study, we asked whether two viral envelope proteins (VSV G and baculovirus GP64) alone encode the signals necessary for the polarized trafficking associated with their respective life cycles. Using *Drosophila* as a model to examine tissue-specific polarized trafficking of these viral envelope proteins, we identified one of the virus-encoded signals and several host proteins associated with regulating the polarized trafficking in the midgut epithelium.

Introduction

To successfully establish a systemic infection in an animal host, most viruses must enter, replicate, and exit from various cell and tissue types. In some tissues, particularly those comprised of polarized cells, entry of the virus and egress of progeny virus particles must be specifically directed to enable successful propagation of the infection within the organism and to new hosts. This is particularly important for arboviruses, viruses that are vectored between different host species. Of critical importance for arboviruses, the virus must transit through two insect tissue barriers: midgut and salivary gland epithelia.

Viruses that infect insects can be subdivided into a) those with simple life cycles requiring only one host to complete their life cycle (*e.g.*, insect-specific viruses) and b) those with complex life cycles requiring more than one host (*e.g.*, arboviruses). Some insect-specific viruses represent important components of ecosystems and may regulate insect populations in nature. One such group, baculoviruses, are virulent pathogens of insects and have been developed as commercial biopesticides to control important pest insect species (1-3). Arboviruses utilize arthropods as vectors to infect vertebrate hosts and can have substantial impacts on human health. Arthropod-transmitted diseases of humans account for roughly 17% of infectious diseases worldwide, with over 3.9 billion people at risk for contracting arbovirus diseases (4-6). A fascinating aspect of arbovirus biology is their ability to infect, replicate, and move between two highly divergent host groups, insects and vertebrates, a process that poses substantial biological challenges.

In the case of both insect-specific viruses and arboviruses, insect infection is typically initiated when orally acquired virus particles infect midgut epithelial cells (7). Viruses enter the polarized midgut cells (enterocytes) from the apical (gut lumen-facing) cell surface and establish a primary infection there. Following viral replication, progeny virions from the primary midgut infection are released from the basal surfaces of enterocytes into the open circulatory system (hemocoel) of the host insect, where they subsequently initiate a secondary round of infection that may include many other tissues. Thus, for systemic infections, the midgut epithelium is a critical early barrier, and efficient basal trafficking and escape are required to establish a robust secondary infection. In the case of arboviruses, secondary infection of the salivary glands is another pivotal component of the lifecycle, one that is required for transmitting the infection to vertebrate hosts. In salivary gland cells, the virus replicates and releases progeny virions into salivary secretions, which the arthropod vector injects into vertebrate hosts during blood feeding. Thus, appropriately

navigating across the polarized cells of both the midgut and salivary glands is necessary to complete the arbovirus life cycle.

The midgut epithelium and salivary glands are structurally complex tissues (8-10) with dramatically different functions in the insect. Typical of most insects, the *Drosophila melanogaster* midgut is comprised of a single layer of polarized epithelial cells, containing four cell types: enterocytes (ECs), enteroendocrine cells (EEs), enteroblasts (EBs), and intestinal stem cells (ISCs) (11). ECs represent the majority of the biomass of the midgut, accounting for approximately 70% of the cells (12). The midgut cells are protected apically by a non-cellular chitinous structure called the peritrophic matrix (PM), which lines the lumen of the midgut. The midgut cells are supported basally by a layer of extracellular matrix called the basal lamina and a layer of visceral muscles surrounding the gut. Midgut ECs typically have small finger-like projections (microvilli) on the apical surface facing the lumen of the gut. The basal surfaces of ECs comprise a tightly folded and relatively thin labyrinth of the basal membrane, which is closely associated with the basal lamina and surrounded by visceral muscle (13). Midgut cells secrete digestive enzymes into the gut lumen, and nutrients absorbed from the gut are transported across the midgut ECs and delivered to the hemocoel. Thus, the polarized midgut cells robustly transport cargos in both directions. Together, the PM, midgut cells, and basal lamina serve as a substantial primary defense against infection by microorganisms.

Similar to the midgut, the salivary glands are also comprised of a single monolayer of epithelial cells, and these cells produce salivary secretions. Salivary secretions facilitate digestion in insects in general, and serve other specialized functions such as delivery of anticoagulants, anesthetics, and vasodilators in blood-feeding insects (14, 15). Similar to the *Drosophila* adult midgut, which is divided into 5 morphologically and transcriptionally distinct regions, the adult salivary gland may be divided into 3 regions that are hypothesized to be responsible for salivary secretion (medial and distal regions) and reabsorption (proximal region) (10, 16, 17).

The mechanisms for directing polarized transport of proteins and budding of virus particles in invertebrate tissues (midgut, epidermis, Malpighian tubules, salivary glands, *etc.*) are largely unknown. While a virus may alter the host cell cytoskeleton (18), organellular membranes (19), endocytic and/or trafficking pathways (20, 21), it is also plausible that polarized trafficking of viral proteins is primarily directed by signals and motifs that interact with existing cellular infrastructure for trafficking through intrinsic host pathways (22, 23). These factors may vary for different virus

groups and for specific proteins. Thus, an important question is whether substantial modifications of cellular architecture or function are necessary for appropriate polarized trafficking of specific viral proteins.

For many insect-specific viruses and arboviruses, virions enter midgut cells from the apical membranes adjacent to the midgut lumen, and progeny are released from basal membranes into the hemocoel, where they circulate and infect a variety of other tissues. In the case of arboviruses, circulating virions enter at the basal surfaces of salivary gland cells, replicate, and progeny virions are released from apical surfaces that interconnect with the salivary gland lumen. Virions in salivary secretions are then delivered to the vertebrate host upon blood feeding. This trafficking scheme represents an enigma: in the midgut, the virus must enter cells apically and release progeny virions basally, whereas in the salivary gland cells, the virus must enter basally and release progeny virions apically. Thus, it appears that arboviruses either differentially modulate trafficking within midgut enterocytes vs. salivary gland cells, or that cellular trafficking pathways may differ significantly in these specialized cell types. It is also possible that some arboviruses may not rely on directional virion release from polarized cells and instead depend on sufficient levels of non-directional virion release. Polarized protein trafficking and virus budding involve many coordinated events, which may include polarized trafficking of: components for nucleocapsid assembly at budding sites and/or pre-assembled nucleocapsids, cellular and/or viral proteins required for fission of host membranes during budding, and viral envelope proteins for display on newly budded virions. Because host membrane proteins can be dramatically segregated on apical or basal membranes of specific polarized cells, viral envelope proteins may utilize existing tissue-specific differences in polarized trafficking pathways to facilitate viral protein trafficking to the appropriate polarized budding sites. Thus, there are many open questions regarding the roles of viral signals and host pathways that direct and regulate polarized protein trafficking and virion egress in critical insect tissues.

In the current study, we used two model viral envelope proteins (baculovirus GP64 and vesicular stomatitis virus glycoprotein G, VSV G) as representatives of insect-specific viruses and arboviruses, respectively, to examine polarized trafficking in two vital insect tissues: midgut and salivary glands. Baculoviruses are virulent pathogens in many lepidopteran species, and their pathology primarily results from systemic infection of most host tissues (24). VSV is an arbovirus that causes blister-like lesions in horses, cattle, swine, and occasionally in humans. VSV is

transmitted to horses and cattle by blood-feeding insects such as biting midges, black flies, sand flies, and possibly mosquitoes (25). For both viruses, the envelope proteins are essential for the production of infectious progeny virions (26, 27). The VSV G protein has been used extensively as a model for protein trafficking in mammalian cells (28), and VSV G is known to be specifically targeted to basal membranes of polarized mammalian MDCK cells (29, 30). However, little or nothing is known regarding the trafficking of VSV G in insect midgut or salivary gland cells. The structure and function of the baculovirus GP64 protein have also been studied extensively in the context of cultured cell infections (26, 31, 32), and basolateral GP64 localization was previously reported in the insect midgut in the context of baculovirus AcMNPV-infected enterocytes (33). Thus, VSV G and GP64 represent excellent models for studies of viral envelope protein trafficking in polarized insect midgut and salivary gland cells.

To investigate trafficking of viral envelope proteins in these polarized tissues, we used the tractable model insect, *Drosophila melanogaster*, to generate a transgenic system for expressing and monitoring viral envelope protein trafficking. We found that expression of either GP64 or VSV G alone was sufficient for the basal trafficking of either protein in midgut enterocytes. In salivary gland cells, GP64 was trafficked basally. In contrast, VSV G was trafficked apically in most salivary gland cells. To explore the mechanisms responsible for polarized trafficking in these key tissues, we first examined a previously identified YxxØ basal trafficking motif that is present in both VSV G and GP64. We found that Alanine substitutions in the YxxØ motif disrupted basal trafficking of both VSV G and GP64 in midgut enterocytes, but had no substantial effect on the trafficking of either VSV G or GP64 in salivary gland cells. Using RNAi in enterocytes, we also examined the roles of clathrin adapter protein (AP) complexes which are known interact with the YxxØ motif, and Rab GTPases which regulate vesicular protein trafficking. To better characterize similarities and differences in trafficking pathways, we also analyzed the localizations of 30 Rab GTPases in midgut and salivary gland cells. We found that AP-1 and AP-3 clathrin adaptor complexes and several Rab GTPases were important for basal VSV G trafficking in enterocytes.

Results

GP64 and VSV G are trafficked basally in *Drosophila* midgut enterocytes independent of viral infection

For viruses that are acquired orally by insects, the midgut is a cellular barrier to systemic infection. Following replication in the midgut epithelial cells (*i.e.* enterocytes or ECs), egress of progeny virions into the hemocoel is critical for initiating the secondary (systemic) phase of infection. Envelope proteins are crucial viral structural components since they are often required for virion assembly and egress, and are necessary for virion binding and entry into host cells (34, 35). Therefore, for many insect viruses, transport of viral envelope proteins to basal membranes of infected midgut enterocytes is essential for efficient assembly and egress of infectious progeny virions. However, it remains unknown whether this requires viral reprogramming of the trafficking pathways in enterocytes, whether these viral proteins utilize existing cell trafficking machinery, or whether they are indeed trafficked basally. We selected two model viral envelope proteins to examine this phenomenon in the insect midgut: GP64 as a representative envelope protein from insect-specific viruses, and VSV G as a representative envelope protein from viruses vectored by insects (arboviruses) (36, 37). GP64 is one of the more intensively studied envelope proteins from insect-specific viruses, and VSV G has served as an important model protein in numerous membrane protein trafficking studies in mammalian cells (26, 38-40).

We first investigated whether VSV G or GP64 would traffic basally in insect midgut enterocytes in the absence of infection. To address this question, we generated transgenic *Drosophila* lines that inducibly express either VSV G or GP64, without any other viral protein(s) that might modify cellular architecture or pathways. We found that both VSV G and GP64 were concentrated in the basal portion of the cells adjacent to the visceral muscles (Fig. 1A, B and Fig. S1A), and that were each displayed on basal enterocyte surfaces of non-permeabilized tissues (data not shown). The basal-most 20% region in the enterocytes accounted for 70.4 ± 1.28% (mean ± SE, n = 96) and 70.3 ± 1.25% (n = 90) of the total VSV G and GP64 signals, respectively (Fig. 2B, Midgut, WT VSV G and GP64). Therefore, the information necessary for basal trafficking in insect midgut enterocytes is encoded in both viral envelope proteins and does not require other viral proteins or infection.

VSV G trafficking in *Drosophila* salivary gland cells differs from that in midgut enterocytes

After exiting infected enterocytes, viruses circulating in the hemolymph infect secondary tissues by interacting with and entering cells via their hemocoel-facing surfaces. The salivary gland is a secondary site of infection and a tissue barrier that is essential for arboviruses to cross for

successful transmission (41). Insect-specific viruses such as baculoviruses may also infect salivary glands, but unlike arboviruses, efficient apical egress of baculovirus progeny virions into saliva is not necessary for their dissemination. Arboviruses, on the other hand, must enter the salivary glands basally but exit apically into the salivary gland lumen, an orientation of transit opposite to that in the midgut epithelium (apical entry and basal exit). Viral envelope proteins of arboviruses may therefore traffic differently in the midgut vs. salivary glands. Because salivary gland epithelial cells have distinctly different cellular architecture and function than midgut enterocytes (Fig. 1A vs. 1C) (10, 17, 42-46), it is unclear whether the same trafficking signals or mechanisms are used in these two barrier tissues. To better understand the differences in the cellular architecture of midgut and salivary gland cells, we examined a series of cellular markers using antibodies and stains that identified proteins associated with apical domains (cortical actin), septate junctions (Discs large), and basolateral domains (E-Cadherin) of polarized cells (Fig. 1 and S2). Midgut epithelial cells (enterocytes) are characterized by apical projections (microvilli; Fig. 1A), and a basal region that is a tightly packed labyrinth of small membrane invaginations (47). In contrast, the polarized salivary gland cells contain large invaginations of the apical surface known as canaliculi that penetrate deep within the cell, and a basal surface that is adjacent to the hemolymph (Fig. 1C). The apical membrane surfaces of the salivary gland cells line the lumen of the canaliculi, which empty into the salivary gland lumen.

We expressed VSV G in salivary gland cells and analyzed its distribution to determine whether VSV G expressed alone is sufficient for its apical trafficking, consistent with the requirements for arbovirus egress. We found that VSV G localized near the apical invaginations in most salivary gland cells (Fig. 1D). However, the observed patterns of VSV G distribution were variable. Patterns among VSV G expressing cells ranged from basally enriched (18.8% of cells) to no polarity (52.5%) to apically enriched (28.8%) (Fig. S3). Salivary gland cells with distinct apical localization of VSV G are highlighted in Figure 1D, and examples of basal and non-polarized distributions in salivary gland cells are shown in Figure S3. Thus, VSV G does not have a consistently polarized distribution in salivary glands, which contrasts with the uniformly basal distribution of VSV G in midgut enterocytes. Despite the variability in VSV G distribution, the majority (81.3%, n = 160) of salivary gland cells showed apical VSV G (Fig. S3, WT). The large proportion of cells exhibiting some apical VSV G suggests that this level of apical trafficking could potentially support egress of the virus from salivary gland cells into saliva for transmission.

We similarly examined the distribution of GP64 expressed in adult *Drosophila* salivary gland cells. In contrast to the variable but frequently apical localization of VSV G, GP64 was consistently concentrated in basal regions of salivary gland cells (Fig. 1D). This basal enrichment of GP64 in the salivary gland cells was similar to that of the midgut enterocytes, with all (100%, n = 163) of the salivary gland cells showing basal GP64 localization.

The divergent trafficking of VSV G in midgut enterocytes and salivary gland cells (basal enrichment in midgut enterocytes and more apical localization in salivary gland cells) parallels the anticipated polarized virion budding in these two tissues. The basal localization of GP64 in both tissues is also consistent with the infection cycle of the insect-specific baculovirus, in which viral egress into the hemocoel facilitates dissemination and systemic infection. In both cases, the interaction of each of these viral envelope proteins with the cell trafficking machinery is sufficient for their appropriate basal or apical trafficking, and reflect key differences between insect-specific and insect-vectored virus movement through their insect hosts.

A YxxØ motif directs polarized trafficking of VSV G and GP64 in *Drosophila* midgut enterocytes

Both VSV G and GP64 are homotrimeric type 1 integral membrane proteins that are functionally and structurally related class III viral fusion proteins (48), despite being from different viral families (ssRNA Rhabdoviridae and dsDNA Baculoviridae, respectively) with dramatically different infection cycles. Since they are both trafficked basally when expressed in uninfected midgut enterocytes (Fig. 1B), they may utilize similar strategies or protein motifs to engage insect host cell basal trafficking machinery in the midgut. VSV G and GP64 both contain a canonical tyrosine-based YxxØ motif (Y = tyrosine; x = any amino acid; Ø = a bulky hydrophobic amino acid) in their short cytoplasmic tails (Fig. 2A). The requisite tyrosine (Y) and isoleucine (I) residues of the VSV G YxxØ motif (YTDI) have previously been identified as necessary for its basal trafficking in polarized mammalian cell cultures (MDCK cells) (29, 30). We therefore hypothesized that the YxxØ motif from VSV G and GP64 might direct basal trafficking of these proteins in *Drosophila* midgut enterocytes *in vivo*. To investigate this, we substituted the Y and I residues in VSV G with alanine (YTDI to aTDa) and incorporated the substituted VSV G construct (VSV $G^{\Delta Y}$) into a transgenic *Drosophila* line (Fig. 2A, VSV G). We also produced a similar GP64 construct in which the corresponding Y and I residues of the putative YxxØ motif of GP64 were

substituted (YCMI to aCMa) and generated a transgenic *Drosophila* line for expressing the modified GP64 ($GP64^{\Delta Y}$) (Fig. 2A, GP64). The fly lines encoding VSV G or GP64 with alanine substitutions were then used to functionally analyze the role of the YxxØ motif for basal trafficking of both proteins in polarized insect midgut enterocytes.

When VSV $G^{\Delta Y}$ was expressed in midgut enterocytes, the dramatic basal localization that was previously observed with the VSV G^{WT} protein was lost (Fig. 2B, Midgut, VSV G, WT vs ΔY). VSV G^{WT} was found concentrated along the basal portion of the cell, suggesting association along the tightly invaginated basal labyrinth, while VSV $G^{\Delta Y}$ was often adjacent to and above nuclei and in the brush border (apical) (Fig. 2B, Midgut, VSV G, ΔY). Similarly, the dramatic basal enrichment of $GP64^{WT}$ was lost when the modified GP64 ($GP64^{\Delta Y}$) was expressed in enterocytes (Fig. 2B, Midgut, GP64, WT vs ΔY). To quantify differences in polarized trafficking patterns between WT and modified VSV G and GP64 proteins, we plotted the mean basal-to-apical distributions of the envelope proteins across numerous cells (see Materials and Methods and Fig. S1). Each graph in Figure 2B displays the relative basal-to-apical distribution of the envelope proteins (*e.g.*, VSV G^{WT} vs. VSV $G^{\Delta Y}$) from 3 separate replicates with approximately 3-5 guts and at least 20 enterocytes per replicate (total $n \geq 69$ per genotype). The VSV G^{WT} localization pattern was strongly basal, with approximately 70.4 ± 1.28% of the signal in the basal-most 20% region of the enterocytes (Fig. 2B, VSV G, WT, open circles). In contrast, VSV $G^{\Delta Y}$ was significantly less basally enriched with only 32.5 ± 1.20% of the signal in the basal-most 20% of the enterocytes (Welch's t-test: $t = 21.6$, $df = 161$, $p < 2.2 \times 10^{-16}$) (Fig. 2B, VSV G, ΔY, filled squares). When the same comparison was performed with $GP64^{WT}$ and $GP64^{\Delta Y}$, a similar loss of basal enrichment of $GP64^{\Delta Y}$ (37.5 ± 1.13% basal signal) was detected when compared to $GP64^{WT}$ (70.3 ± 1.25% basal signal) ($t = 19.4$, $df = 188$, $p < 2.2 \times 10^{-16}$) (Fig. 2B, GP64, WT vs ΔY). $GP64^{\Delta Y}$ signals were more diffuse within cells compared to $GP64^{WT}$, and $GP64^{\Delta Y}$ was sometimes detected in the apical brush border. These data indicate that the YxxØ motif in the cytoplasmic tails of both VSV G and GP64 are functional motifs required for the basal trafficking of both viral envelope proteins in polarized insect midgut enterocytes.

The YxxØ motif is not a prime determinant of polarized trafficking of VSV G or GP64 in *Drosophila* salivary gland cells

Our prior analysis of protein markers of cell polarity showed that the apical-basal orientation of midgut enterocytes and salivary gland cells were similar, with basal membranes adjacent to the hemocoel and the apical membranes bordering the lumen of the organ. To determine whether alteration of the YxxØ motif would impact VSV G trafficking in salivary gland cells, we compared the distribution patterns of VSV G^{WT} and VSV $G^{\Delta Y}$. Tyrosine motif disruption resulted in slightly reduced basal VSV G localization, with the basal-most 20% region of the salivary gland cells accounting for 23.4 ± 0.97% of the total VSV G^{WT} signal and 13.8 ± 0.56% of the total VSV $G^{\Delta Y}$ signal (Wilcoxon rank-sum test: w = 25056, $p = 1.33 \times 10^{-15}$), but did not change the overall distribution pattern and only slightly increased VSV G localization in the apical-most 40% region of the salivary gland cells (49.5 ± 1.13% to 53.2 ± 0.79%, t = -2.62, df = 298, $p = 9.25 \times 10^{-3}$) (Fig. 2C, VSV G, graph). Thus, ablation of the YxxØ motif did not result in a substantial change in the overall distribution pattern (Fig. 2C, VSV G, graph; and Fig. S3), suggesting limited involvement of the YxxØ motif in the apical trafficking of VSV G in salivary gland cells. It is important to note that since apical membranes of salivary gland cells extend deep into the cytoplasm (Fig. 1C), our method for quantifying basal-to-apical distribution in salivary gland cells may underestimate apical enrichment of VSV G (*i.e.*, VSV G decorating the apical membrane reaching the level of the nucleus would not appear apical in the graphs). Nevertheless, our results indicate that VSV G is apically localized in most salivary gland cells, and the VSV G YxxØ motif appears to play only a minimal role in its apical trafficking in *Drosophila* salivary gland cells.

In contrast to the apical distribution of VSV G^{WT} in the salivary gland cells, $GP64^{WT}$ was concentrated basally in salivary gland cells (Fig. 2C, GP64). This localization of GP64 was similar to that observed in midgut enterocytes (Fig. 2B vs. 2C, GP64). The basal enrichment of $GP64^{\Delta Y}$ was only marginally reduced in the basal-most 20% region of the salivary gland cells when compared to $GP64^{WT}$ (52.3 ± 1.55% for $GP64^{\Delta Y}$ vs 56.8 ± 1.53% for $GP64^{WT}$, w = 17017, p = 0.048) with no influence on the overall distribution pattern (Fig. 2C, GP64, graph). This suggests minimal involvement of the YxxØ motif in the basal trafficking of GP64 in the salivary gland cells.

Altogether, our data suggest that while the YxxØ motifs are required for basal trafficking in midgut enterocytes, they are mostly dispensable for directing trafficking of either GP64 or VSV G in salivary gland cells. Furthermore, the observation that VSV G is found apically in salivary gland cells while strictly basal in enterocytes, whereas GP64 is strongly basal in both tissues,

indicates that there are additional, yet unidentified trafficking/sorting motifs in VSV G and GP64, as well as differences in the mechanisms of polarized trafficking between midgut enterocytes and salivary gland epithelial cells. Both aspects are topics of interest for future studies.

Clathrin AP complexes 1 and 3 direct basal trafficking of VSV G in *Drosophila* midgut enterocytes

We next focused on the identification of key host factors involved in the basal trafficking of viral envelope proteins in midgut enterocytes. Clathrin adaptor protein (AP) complexes direct a large variety of membrane trafficking events in the cell. This may include trafficking among compartments (ER, Golgi, endosomes, lysosomes, *etc.*) as well as polarized and non-polarized trafficking to subdomains of the plasma membrane. *Drosophila* encodes 3 AP complexes (AP-1, AP-2, and AP-3) and each is a heterotetrameric assembly composed of two large subunits (γ/α/δ/ε/ζ or β), a medium subunit (μ), and a small subunit (σ). In models of polarized trafficking of membrane proteins in mammalian cells, interactions between membrane protein YxxØ motifs and the μ subunits of clathrin AP complexes are early steps in protein trafficking to basal membranes. Also, in a prior RNAi screen of cultured *Drosophila* cells (31), we found that RNAi of clathrin (*chc*) and AP genes (*AP-2μ* and *AP-1,2β*) resulted in decreased GP64 transport to the cell surface. Although AP-1,2β is not expected to directly interact with the YxxØ motif, depletion of any one of the four canonical subunits of an AP complex is expected to render its corresponding complex nonfunctional. In *Drosophila* and other insects, AP-1,2β is shared between the heterotetrameric AP-1 and AP-2 complexes, both of which would therefore be inactivated upon AP-1,2β RNAi. Since we identified the importance of the YxxØ motif in the basal trafficking of VSV G in midgut enterocytes, we next examined the roles of the three AP complexes in the polarized transport of VSV G in that tissue.

To probe the role of each AP complex, a fly line (*Myo-GAL4, UAS-nlsGFP, tub-GAL80^{ts}; UAS-VSV G^{WT}*) with temperature-regulated midgut expression of VSV G^{WT} was crossed with RNAi lines to obtain F1 progeny co-expressing VSV G and an RNAi construct targeting (separately) each one of three clathrin adaptor complexes. We then compared VSV G distribution patterns in each of the AP complex RNAi flies to negative controls (midguts from driver/*AttP2* background control, lacking any RNAi). VSV G showed strong basal enrichment in enterocytes of control midguts (Fig. 3, top panels). However, when VSV G was co-expressed with RNAi

constructs that targeted AP-1μ or AP-3μ, the strong basal localization of VSV G was lost, and VSV G was distributed less basally (32.3 ± 0.771% and 45.2 ± 1.39%, respectively) compared to the control (56.9 ± 1.06%) in the basal 20% region of the enterocytes (Pairwise Wilcoxon rank sum test: $p < 2.00 \times 10^{-16}$ and $p = 6.00 \times 10^{-9}$, respectively) (Fig. 3, Control vs. AP-1μ and AP-3μ). This contrasts with the result from the RNAi of AP-2μ (53.2 ± 1.38%), in which VSV G distribution appeared similar to that of control enterocytes (56.9 ± 1.06% basal) ($p = 0.126$) (Fig. 3, Control vs. AP-2μ). The patterns observed in the presence of AP RNAi targeting AP-1μ or AP-3μ were similar to that observed when the YxxØ motif was ablated in construct VSV $G^{\Delta Y}$ (Fig. 2B, VSV G, ΔY). These patterns were consistent across independent midguts (≥ 3) and individual cells ($n \geq 119$) after 3 days of RNAi. We also observed a similar disruption of basal trafficking from an RNAi line targeting AP-1,2β (40.4 ± 0.958%), which served as a positive control ($p < 2.00 \times 10^{-16}$) (Fig. 3, Control vs. AP-1,2β). In addition to the above results, pharmacological disruption of the YxxØ-AP interactions using anthranilic acid (ACA) (49) reduced VSV G^{WT} localization in the basal-most 20% region of midgut enterocytes (65.4 ± 1.97% in control vs. 50.4 ± 1.53% in ACA treated; $w = 4154$, $p = 3.48 \times 10^{-8}$) (Fig. S4). Thus, our results from RNAi of AP complexes combined with results from YxxØ ablation in VSV G, and exposing flies to ACA suggest that AP-1 and AP-3 but not AP-2 complexes are necessary for YxxØ-mediated VSV G basal trafficking in midgut enterocytes.

Specific Rab GTPases are important for basal trafficking of VSV G in *Drosophila* midgut enterocytes

Rab GTPases are known to be master regulators that direct vesicular protein sorting and trafficking. Their numerous roles include the regulation of vesicle budding, transport, tethering, and fusion with target membranes (50). Specific Rab GTPases may also serve different roles in different cell types (51). Importantly, they have also been shown to be required for basal trafficking of host and viral proteins (52-58). Rab GTPases are engaged in the establishment and maintenance of cell polarization (59, 60) and the specific subcellular localization of some Rab GTPases may differ in different cell types or tissues. To identify Rab GTPases that could be involved in the basal trafficking of VSV G in enterocytes, we first selected two groups of candidate Rab genes: (1) Rab GTPases that have previously been shown to be important for viral protein trafficking in other cellular systems and (2) Rab GTPases that showed divergent apical-basal localization patterns in

enterocytes compared to salivary gland cells. For the first group, we had previously identified Rab1 and 4 as essential for the transport of GP64 to the surface of non-polarized cultured *Drosophila* cells (31). Although we did not identify Rab11 as important in that study, we included Rab11 in the current study due to its involvement in sorting/recycling endosome function, similar to Rab4, which was important for GP64 surface trafficking (31, 61). It was previously shown that basal trafficking of VSV G in mammalian MDCK cells requires coordination of the AP-1 complex with Rab8 (53) and that Rab10 is required for basal secretion of *Drosophila* gut basal lamina components (57). Therefore, we investigated whether Rab1, 4, 8, 10, and 11 play any roles in basal VSV G trafficking in insect midgut enterocytes. To select a second group of candidate Rab GTPases, we performed a comprehensive comparative analysis of the localization patterns of 30 YFP-tagged Rab GTPases (62) in *Drosophila* midgut enterocytes and salivary gland cells (Fig. S5). For this analysis, UAS-driven YFP-tagged Rab GTPases were ubiquitously expressed under the *da-GAL4, tub-GAL80^{TS}* driver and we compared the distribution of each YFP-tagged Rab GTPase in midgut vs salivary gland cells by confocal microscopy. We identified several YFP-Rab GTPases with basal enrichment (Rab8, 10, and 30) or both basal and apical enrichment (Rab23 and 35) in enterocytes, but with salivary gland cell localization patterns that differed from that of midgut enterocytes; either apically enriched in the canaliculi (Rab23 and 35) or in a non-polarized localization pattern (Rab8, 10, and 30).

Next, we examined these selected Rab GTPases to assess their potential roles in basal trafficking of VSV G in *Drosophila* midgut enterocytes. We co-expressed VSV G with RNAi constructs that separately targeted each of the following Rab GTPases: Rab1, 4, 8, 10, 11, 23, 30, or 35 (Fig. 5) by crossing with a fly line with temperature-regulated VSV G midgut expression (*Myo-GAL4, UAS-nlsGFP, tub-GAL80^{ts}; UAS-VSV G^{WT}*). F1 progeny flies were shifted to the permissive temperature to allow co-expression of VSV G and Rab RNAi for 5 days (with the exception of Rab11 RNAi, which was co-expressed with VSV G for only 3 days to avoid gut dysplasia) before dissecting and immunostaining midgut enterocytes to assess VSV G localization. Basal enrichment of VSV G was significantly reduced in midgut enterocytes of flies co-expressing VSV G and each of the RNAi constructs targeting: Rab1 (42.2 ± 0.889%), Rab4 (42.8 ± 0.705%), Rab8 (36.6 ± 0.884%), Rab10 (39.1 ± 1.16%), Rab23 (41.8 ± 0.884%), Rab30 (41.6 ± 1.07%), and Rab35 (44.7 ± 1.08%) compared to their respective controls (Attp2 for Rab1, 4, 8, and 10: 53.7 ± 0.980%; Attp40 for Rab23 and 35: 56.3 ± 0.839%; and Attp2 for Rab30: 56.9 ± 1.06%) (Pairwise

Wilcoxon rank sum test: $p = 3.9 \times 10^{-14}$, $p = 3.4 \times 10^{-14}$, $p < 2.0 \times 10^{-16}$, $p = 5.2 \times 10^{-16}$, $p < 2.0 \times 10^{-16}$, and $p = 1.3 \times 10^{-14}$, respectively for each Rab RNAi compared to its control) (Fig. 5, graph). Surprisingly, we found no substantial effect on VSV G basal localization from Rab11 RNAi (79.1 ± 1.12%) compared to the control (78.0 ± 1.32%) ($w = 7547$, $p = 0.665$) (Fig. 5, Control vs. RNAi Rab11). Thus, our analysis revealed that all but one of the Rab GTPases selected for analysis (Rab1, 4, 8, 10, 23, 30 and 35) appear to be involved in basal trafficking of VSV G in midgut enterocytes. While RNAi has been used extensively, it is important to note the substantial limitations of this indirect technique. Although the Rab GTPase RNAi phenotypes (disrupted basal VSV G trafficking in ECs) mirror those observed for the ΔY VSV G protein, we cannot fully assign direct roles to the identified Rab GTPases, due to their many and coordinated functions in cells. Further studies will be required to explore the direct or indirect roles of these Rab GTPases.

Discussion

Viral trafficking within insect hosts is critical for the success of the viral life cycle. Because little is known about how insect viruses navigate across important tissue barriers in their insect hosts, we examined the subcellular trafficking of two model viral envelope proteins in two critical barrier tissues: midgut and salivary glands. In addition to their roles as barriers and bottlenecks to virus infection and transmission, midgut and salivary glands serve distinct physiological roles in insects. The midgut is the primary tissue for absorption of nutrients and their transfer to the circulatory system. As such, the protein trafficking pathways in the midgut are specialized for apical secretion of digestive enzymes and components of the peritrophic matrix, as well as for absorption of nutrients from the gut lumen. Absorbed nutrients are transported to the basal surfaces of midgut enterocytes, where they are delivered to the hemocoel. In addition, the basal lamina, a thick collagen-containing matrix, is secreted from the basal surfaces of midgut enterocytes. Thus, protein transport and secretory pathways within midgut enterocytes perform many central functions that require precise recognition of proteins and targeted polarized transport. Insect salivary glands produce secretions that play roles in feeding, particularly in food processing (pre-digestion, lubrication) and sometimes in manipulation of the host during blood feeding (anticoagulation, anesthesia, vasodilation, *etc.*). In some insects, such as mosquitoes, salivary gland cells secrete large quantities of saliva, which is stored in large apical cavities (acinar cavities) (17, 42, 44, 63). In other insects, such as blow flies, the apical membrane of the salivary gland cells forms deep invaginations (canaliculi) that greatly increase membrane surface area for

459 secretion (64). As such, the salivary glands represent a robust secretory and release apparatus, but
460 the cellular architecture (invaginated apical membranes) and cell types (the lack of visceral
461 muscles and stem cells) differ fundamentally from that of the midgut. Many viruses that infect
462 insects have adapted to utilize the complex transport systems in various cell types to move
463 infection through the animal successfully. Such navigation of viral infection through the animal is
464 particularly interesting in the case of arboviruses, but it is also crucial for the success of insect-
465 pathogenic viruses.

466 To examine viral envelope protein trafficking through these polarized tissues of insects,
467 we used transgenic *Drosophila* to express genes encoding either baculovirus (AcMNPV) GP64 or
468 an arbovirus (VSV) G in these tissues. Upon expression, each viral envelope protein was
469 transported to and concentrated in the basal region of midgut enterocytes (Fig. 1), and was
470 displayed on basal surfaces, even though no other viral proteins were present. This result mirrors
471 the basal envelope protein trafficking reported during infections (VSV-infected MDCK cells and
472 AcMNPV-infected *T. ni* midgut) (29, 30, 33), and demonstrates that the information required for
473 polarized envelope protein trafficking in insect midgut enterocytes is encoded within the GP64
474 and VSV G proteins.

475 We also examined polarized trafficking of these proteins in salivary gland cells. Salivary
476 gland cells are specialized for secreting proteins into the lumen of the salivary glands. Arboviruses
477 utilize salivary gland trafficking pathways to exit the insect vector host and facilitate infection of
478 the vertebrate host during blood feeding. Because this viral transit appears to be in an orientation
479 that is opposite to that observed in midgut enterocytes, we first used a series of polarity markers
480 to determine the apical-basal orientation of cells within the salivary gland epithelium (Fig. S2).
481 We confirmed that apical membrane domains face the lumen of the salivary glands, and basal
482 membranes are adjacent to the hemocoel. We show that GP64 was consistently localized to basal
483 regions of salivary gland cells, similar to the results from midgut enterocytes (Fig. 1D, GP64). In
484 contrast, yet consistent with the arbovirus life cycle, we found that VSV G was trafficked to the
485 apical invaginations of salivary gland cells (Fig. 1D, VSV G). While VSV G trafficking was not
486 strictly apical in all cells, we found that 28.8% of salivary gland cells had distinctly apical
487 trafficking, while another 52.5% of cells had non-polarized trafficking, and thus some apical
488 presence of VSV G (Fig. S3). This suggests VSV G was trafficked apically in approximately 81%
489 of salivary gland cells, which in the context of a virus infection could effectively promote apical

budding of progeny virions. The observed partial or inconsistent polarized trafficking may indicate that viral infection could provide additional factors necessary for robust apical trafficking of G in salivary gland cells. It is also possible that partial apical trafficking in salivary gland cells is sufficient for VSV transmission, and basal trafficking in salivary gland cells may also play a role in the infection cycle. It is of note that some alphaviruses have been observed to bud into both acinar cavities and from lateral and basal membranes of infected mosquito salivary gland cells (42, 63). While we have focused on a powerful model insect for the current studies, it will be of great interest to examine viral envelope protein trafficking in mosquitoes and other natural hosts. Most importantly, our results show that when GP64 or VSV G was expressed alone, the polarized trafficking of each protein was sufficient to reach polarized locations in cells appropriate to the infection cycles of their parent viruses. These results from *Drosophila* tissues also suggest that the polarized trafficking pathways in midgut and salivary gland cells are widely conserved in insects and that the signals for appropriate polarized trafficking are largely if not entirely encoded in the protein sequences or structures of these viral envelope proteins.

In prior studies of VSV G trafficking in mammalian MDCK cells, a YxxØ (YTDI) amino acid sequence motif in the cytoplasmic tail was identified as necessary for its basolateral targeting (29, 30). When examined in insect midgut enterocytes, we found that alanine substitutions of the key residues in the YxxØ motif resulted in disruption of polarized trafficking, and we concluded that the YxxØ motif is necessary for basal trafficking of VSV G in *Drosophila* midgut enterocytes (Fig. 2). In parallel experiments, we identified a similar YxxØ (YCMI) motif in the GP64 cytoplasmic tail and found that it was also necessary for basal trafficking. Thus, for both VSV G and baculovirus GP64, the YxxØ motif appears to play a critical role in directing polarized trafficking in *Drosophila* midgut enterocytes (Fig. 2B). Surprisingly, when the same modified VSV G and GP64 constructs (containing an ablated YxxØ motif) were examined in salivary gland cells, we observed no substantial effect on polarized trafficking there (Fig. 2C). While the YxxØ motif is necessary in the midgut epithelium, other signals or motifs appear to be required for polarized trafficking in the salivary gland cells. Thus, the pathways or mechanisms involved in VSV G trafficking appear to differ in the midgut enterocytes and salivary gland cells.

In prior studies of cultured mammalian cells, the YxxØ motif was shown to interact with clathrin adapter protein (AP) complexes to direct basal membrane targeting of proteins. (65-69). In mammals and plants, there are five different AP complexes, whereas in *C. elegans,* yeast, and

Drosophila, there are three (70). We therefore examined the role of each of the 3 AP complexes from *Drosophila* in basal trafficking of VSV G in insect enterocytes. Using RNAi of the μ subunit of each complex (the subunit that binds the YxxØ motif), we found that disruption of either the AP-1 or AP-3 complex resulted in disruption of basal trafficking of VSV G in midgut enterocytes (Fig. 3). Furthermore, RNAi of AP-1,2β (which is a beta adaptin shared by the AP-1 and AP-2 heterotetrameric complexes in *Drosophila* (70)), resulted in disrupted VSV G basal trafficking. Importantly, the effects of these specific AP complex RNAi were similar to the effects observed from the ablation of the YxxØ motif in the VSV G protein (Fig. 2B vs. 3).

The AP-1 complex localizes to the trans-Golgi Network (TGN) and recycling/sorting endosomes, and is known to direct clathrin-coated vesicular traffic bidirectionally between these compartments and to basolateral plasma membranes (71). Similar to AP-1, the AP-3 complex is also found on endosomal membranes and the TGN, but in discrete sites that are not overlapping with AP-1. AP-3 has been reported to be involved in cargo transport from early to late endosomes, in the production of lysosome-related organelles in epithelia (65), and in the release of exosomes from neurons (72). The basal trafficking of VSV G in midgut epithelium was not substantially affected when the AP-2 complex was disrupted (Fig. 3), consistent with the typical role of the clathrin AP-2 complex in directing protein recycling from the plasma membrane. Although VSV G, like other YxxØ-motif-containing proteins (73-75), has the potential to be recycled from the plasma membrane to internal organelle membranes, we did not observe an impact on VSV G basal localization in enterocytes when the AP-2 complex was disrupted.

Rab GTPases are key regulators of vesicular trafficking, and we therefore examined selected Rab GTPases for their roles or requirements in basal trafficking of VSV G in insect midgut enterocytes. To better understand how the trafficking pathways might differ in midgut enterocytes and salivary gland cells, and to select Rab GTPases for genetic analysis, we used a bank of fly lines expressing Rab-YFP constructs to map and compare Rab localization in midgut enterocytes and salivary gland cells. We identified eight Rab GTPases (Rab1, 4, 8, 10, 11, 23, 30, and 35) that were either differentially localized in cells of the two tissues (Fig. 4 and S5) and/or predicted to be involved in basal trafficking from studies in other systems. We selected these eight Rab genes for analysis by RNAi. We found that RNAi of Rab1, 4, 8, 10, 23, 30, and 35 resulted in substantial reductions in basal localization of VSV G compared to the control (Fig. 5). In the case of Rab11 RNAi, VSV G localization was similar to that of the control (Fig. 5).

552 Certain Rab GTPases (Rab4, 8, 10) identified here have been previously associated with
553 basolateral trafficking and/or coordination with clathrin AP complexes (76). Rab4 is a component
554 of the sorting/recycling endosome, and VSV G has been reported in some mammalian cells to
555 require recycling endosomes for its delivery to the plasma membrane (77). In midgut enterocytes,
556 it is unclear whether Rab4 is required for the direct basolateral trafficking of VSV G to the plasma
557 membrane, its recycling, or both. Rab4 and 11 have been identified as regulating distinct "fast"
558 and "slow" recycling pathways, respectively (78). Because the Rab11 RNAi did not appear to
559 affect VSV G basal trafficking, we conclude that if recycling is involved in basal trafficking, it is
560 likely due to a Rab4-dependent slow pathway, and the Rab11-based pathway may not play a
561 substantial role. Rab8 depletion has been shown to affect basolateral trafficking of VSV G in
562 mammalian MDCK cells (53). When Rab8 was depleted, it was reported that only basolateral
563 trafficking of VSV G through the secretory pathway (and not through a recycling pathway) was
564 disrupted (52). When we depleted Rab8 in insect midgut enterocytes, VSV G basolateral
565 trafficking was disrupted, resulting in reduced basal VSV G distribution like that observed from
566 Rab1 and Rab4 depletion (Fig. 5). This is consistent with results from another study that found
567 Rab8 to be critical for basolateral trafficking of basal lamina (BL) constituents (collagen IV) in
568 polarized *Drosophila* follicular epithelium. In addition, RNAi targeting Rab10 disrupted basal
569 enrichment of VSV G. Rab10 was also previously shown to aid in directing basolateral trafficking
570 of *Drosophila* follicular basal lamina components (57). Thus, several Rab GTPases identified in
571 our localization mapping and RNAi knockdowns have been identified as important for basal
572 trafficking of host cell proteins in other epithelial cell types.
573 In the case of most insect pathogenic viruses, such as baculoviruses, the secondary
574 infection of many tissues leads to the death of the insect, and progeny virions are liberated from
575 the insect carcass. For arthropod-vectored viruses, progeny virions produced during secondary
576 infection of salivary glands must be released apically into the lumen to facilitate transmission to
577 vertebrate hosts through blood feeding. This divergent scenario of the apical release of virions
578 from salivary glands, relative to the basal virion release from enterocytes, was reflected by apical
579 (or non-polarized) trafficking of VSV G in salivary glands and basal trafficking of VSV G in insect
580 midgut enterocytes (Fig. 1B and 1D). Although VSV G was enriched at the basal-most
581 compartment of some salivary gland cells, a substantial percentage of cells exhibited strongly
582 apical VSV G enrichment in the canaliculi of salivary gland cells (Fig. S3). This demonstrates that

583 apical VSV G trafficking occurs in these cells in the absence of viral infection. This divergent
584 midgut vs. salivary gland VSV G trafficking pattern, combined with differences in Rab GTPase
585 localization patterns in the two tissues, provides substantial evidence that the composition or
586 function of trafficking machinery differs in midgut enterocytes and salivary gland epithelial cells.
587 Interestingly, GP64 expressed in salivary gland cells was not trafficked apically (as observed for
588 VSV G) but localized basally as observed in midgut enterocytes (Fig. 1B and 1D; VSV G vs.
589 GP64). Polarized budding of baculovirus virions has not been previously studied in insect salivary
590 glands, but our observation of GP64 trafficking in *Drosophila* salivary glands suggest that
591 baculovirus virions may be released from basal membranes of the salivary glands to supplement
592 the systemic infection in these insect-specific pathogens. It is also of note that mutation of the
593 YxxØ motif in both VSV $G^{\Delta Y}$ and $GP64^{\Delta Y}$ did not substantially affect the polarized trafficking
594 pattern of either protein in salivary gland epithelium, in contrast to the effects observed in midgut
595 enterocytes (Fig. 2B and 2C). Combined with observed differences in Rab localization patterns in
596 midgut vs. salivary gland cells, this indicates that insect salivary gland cells may have a
597 functionally different membrane protein trafficking network compared to insect midgut
598 enterocytes. The observation that WT VSV G and GP64 traffic in opposite directions in salivary
599 gland cells, while both were minimally affected by mutation of the YxxØ motif in salivary glands,
600 also indicates that there are likely divergent, but yet unidentified, trafficking signals embedded
601 within the VSV G and GP64 sequences or structures.
602 In the current studies, we examined two critical issues in virus interactions with their insect
603 hosts: 1) how viruses (insect-specific and insect-vectored) navigate through the polarized midgut
604 epithelium, the first cellular barrier, to establish systemic infection in the insect host; and 2) how
605 arboviruses move across a second polarized epithelial cell barrier (salivary gland cells) in an
606 opposite direction. To address these issues, we developed and used a powerful genetic system to
607 specifically examine: a) viral envelope protein trafficking in each of these tissues, b) viral protein
608 encoded signals for directing polarized trafficking in both tissues, and c) host cell factors necessary
609 for mediating the polarized trafficking of a viral envelope protein in midgut cells. We found that
610 VSV G and GP64 each encode the signals required for basal trafficking in the midgut epithelium,
611 a necessity for virus budding into the hemocoel and establishing systemic infection. In addition,
612 we found that VSV G was apically trafficked in the salivary gland cells, a process important for
613 virus egress into the saliva. We found that a YxxØ motif was necessary for basal trafficking of

both proteins in midgut enterocytes, but was largely dispensable in salivary gland cells for apical VSV G trafficking and basal GP64 trafficking. By examining host proteins potentially involved in protein trafficking in polarized cells, we identified clathrin adapter complexes AP-1 and AP-3, as well as seven Rab GTPases (Rab1, 4, 8, 10, 23, 30, and 35) that are important for directing basal trafficking of VSV G in polarized midgut enterocytes. While we have developed a new genetic system for these studies and answered several important fundamental questions regarding viral envelope protein trafficking in these two critical tissues that serve as important barriers to systemic infection and transmission, our studies also raise many new questions regarding the mechanisms by which insect-specific viruses and arboviruses interact with and navigate through the tissues of their insect hosts.

Materials and Methods:

Fly transgenesis

Drosophila fly lines encoding either WT VSV G (VSV G^{WT}), WT GP64 ($GP64^{WT}$), modified VSV G (VSV $G^{\Delta Y}$) or modified GP64 ($GP64^{\Delta Y}$) were generated by inserting the WT or modified ORFs downstream of the upstream activation sequence (UAS) in the *Drosophila* transformation plasmid pUASt (*Drosophila* Genomics Resource Center plasmid #1000). The VSV G^{WT} open-reading frame (ORF) was PCR amplified from VSVG-BP95NOTSV (kindly provided by F. M. Boyce) using primers (containing the EcoRI or XbaI sites underlined): forward 5'-AAAGAATTCTGACACTATGAAGTGCCTTTTGTACTTAGC-3' and reverse: 5'-AAATCTAGATTACTTTCCAAGTCGGTTCATCTC-3' and cloned into EcoRI/XbaI sites of pUASt, generating pUAST-VSV G. The modified VSV $G^{\Delta Y}$ ORF contained Y501A and I504A substitutions and was generated by PCR from the VSV G^{WT} template, using the forward primer (containing the EcoRI site underlined): 5'-AAAGAATTCTGACACTATGAAGTGCCTTTTGTACTTAGC-3' and the reverse primer: 5'-CGGTTCATCTC**AGC**GTCTGT**AGC**AATCTGTCTTTTCTTGGTGTGC-3' (mutagenic codons in bold). This primary PCR amplicon was used directly as template for a secondary PCR using the same forward primer and a reverse primer containing an XbaI site (underlined): 5'-AAATCTAGATTACTTTCCAAGTCGGTTCATCTC**AGC**GTCTG-3', then EcoRI/XbaI cloned into pUASt to generate pUASt-VSV $G^{\Delta Y}$. The $GP64^{WT}$ ORF was PCR amplified from AcMNPV

genomic DNA using the forward primer (containing an XbaI site, underlined): 5'-AAATCTAGAATGGTAAGCGCTATTGTTTTATATGTGC-3' and the reverse primer (containing an XbaI site, underlined): 5'-AAATCTAGAATATTGTCTATTACGGTTTCTAATCATACAG-3' and XbaI-cloned into pUASt to generate pUASt-GP64. The mutant GP64$^{\Delta Y}$ ORF, encoding the Y502A and I505A codon substitutions, was generated by PCR. A primary PCR amplicon was generated from the pUASt-GP64^{WT} template using the forward primer (containing an XbaI site, underlined): 5'-AAATCTAGAATGGTAAGCGCTATTGTTTTATATGTGC-3' and the reverse primer: 5'-**AGC**CATACA**AGC**CAAAAATAAAATCACAATTAATATAATTACAAAGTTAACTAC-3' that introduced both alanine mutagenic codons (in bold). This primary PCR amplicon was used directly as template for a secondary PCR using the same forward primer: 5'-AAATCTAGAATGGTAAGCGCTATTGTTTTATATGTGC-3' and the reverse primer (containing an XbaI site, underlined): 5'-AAATCTAGATTAATATTGTCTATTACGGTTTCT**AGC**CATACA**AGC**CAAAAATAAAATCAC-3' (mutagenic codons in bold). High fidelity KOD DNA polymerase (Takara) was used to amplify the entire VSV G and GP64 ORFs (WT and ΔY), which were verified by Sanger sequencing. The resulting pUASt-based plasmids containing the VSV G or GP64 fragments were injected into w^{1118} flies (BestGene Inc, California), and transgenic fly lines were verified for expression of the viral envelope proteins (WT and ΔY versions of VSV G and GP64) by immunoblot analysis. A single transgenic line (expressing each WT or ΔY version of VSV G or GP64) was selected and used for all experiments. The 3' ends of the VSV G and GP64 ORFs were PCR-amplified (using Taq polymerase, NEB) from DNA isolated from each fly line, and the PCR amplicons were sequenced to verify the WT and ΔY forms of cytoplasmic domain sequences for each line from VSV G or GP64.

Fly husbandry and genotypes

All *Drosophila* used in this study were maintained on artificial diet (Table S1) at room temperature (~23°C) under a 12L:12D light cycle unless otherwise indicated. Localization patterns of the WT and alanine-substituted forms of VSV G and GP64 or YFP-Rab GTPases in *Drosophila* midgut enterocytes and salivary gland cells were assessed in the F1 offspring of *da-GAL4, tub-GAL80^{ts}* female ubiquitous driver flies crossed with male flies carrying WT or modified *UAS-GP64 or*

675 *UAS-VSV G. Myo-GAL4, UAS-nlsGFP, tub-GAL80^{ts}; UAS-VSV G^{WT},* and *Myo-GAL4, UAS-*
676 *nlsGFP, tub-GAL80^{ts}; UAS-GP64^{WT}* midgut-specific female driver lines were crossed with male
677 UAS-regulated RNAi and control lines for quantifying VSV G basal-to-apical distribution in the
678 midgut enterocytes. The F1 progeny were allowed to develop at 18°C. F1 adults (3 to 7 days post-
679 emergence) were then incubated at 29º C for 3 or 5 days to induce transgene expression prior to
680 tissue dissection for processing and microscopy. The incubation time at 29°C in each case was
681 carefully selected to avoid gut dysplasia while maximizing the duration of RNAi induction (79).
682 Control AttP2 (36303), AttP40 (36304), and UAS-regulated RNAi lines were obtained from the
683 Bloomington *Drosophila* Stock Center (BDSC): Rab1 (34670). Rab4 (33757), Rab8 (34373),
684 Rab10 (26289), Rab11 (27730), Rab23 (55352), Rab30 (31120), Rab35 (80547), AP-1μ (27534),
685 AP-1,2β (28328), AP-2μ (28040), and AP-3μ/cm (27282). A fly line ubiquitously expressing E-
686 Cadherin-GFP used in the cell polarity markers analysis was generously provided by Bruce Edgar
687 (University of Utah).
688
689 **Immunostaining and Microscopy**
690 Flies were anesthetized on ice before brief immersion in 70% ethanol to remove cuticular
691 hydrocarbons, then transferred to PBS (pH 7.4) in a 9-well glass spot plate. Midguts and salivary
692 glands were dissected in PBS and immediately transferred to 1 ml of 4% paraformaldehyde in PBS
693 (pH 7.4) at room temperature (RT) for 1 h of fixation. Tissues were rinsed (3x, 10 min each at RT)
694 with 1 ml of PBS-T (PBS pH 7.4 containing 0.1% Triton X-100) for cell permeabilization and
695 blocked in 3% BSA in PBS (pH 7.4) for a minimum of 3 h before incubation with primary
696 antibodies (1:1000) in 1% BSA in PBS overnight at RT. Primary antibodies were removed and
697 tissues were washed (3x, 10 min each at RT) with 1 ml PBS-T. Washed tissues were incubated in
698 secondary antibodies (1:1000) and Alexa Fluor 555 phalloidin (1:1000) (Invitrogen) in 1% BSA
699 in PBS (pH 7.4) for 2-4 h in darkness at RT. Secondary antibodies were removed, and tissues were
700 washed (3x, 10 min each at RT) with PBS, then stained in 1 ml of 0.5 μg/ml DAPI (Sigma-Aldrich)
701 in PBS for 30 min at RT in darkness, then washed (3x for 10 min at RT) with PBS. Stained tissues
702 were mounted onto slides in glycerol-based, aqueous mounting media containing an antifadent
703 (Citifluor AF3). Tissues in mounting media were placed between pedestals consisting of two layers
704 of double-sided Scotch tape to prevent crushing of the tissues by the coverslip. The enterocytes of
705 midgut region 2 and the secretory cells of the medial salivary gland were analyzed in this study.

Slides were imaged on a Zeiss 710 confocal microscope using the 40x or 63x oil immersion objectives. Primary antibodies used for immunostaining were directed against: AcMNPV GP64 (AcV5), VSV G (8G5F11, generous gift from Gary Whittaker, Cornell University), Discs large (DSHB 4F3), GFP (Invitrogen, A10262), Integrin β1 (DSHB 7E2), Snakeskin, and Tetraspanin 2A (Generous gifts from Mikio Furuse, National Institute for Physiological Sciences, Japan). Alexa Fluor 647 donkey anti-mouse, Alexa Fluor 555 donkey anti-rabbit, and Alexa Fluor 488 goat anti-chicken secondary antibodies (Invitrogen) were used in this study.

VSV G and GP64 protein distribution in fly tissues

VSV G and GP64 signal distributions in immunostained tissues were determined using ImageJ (v.1.53c). To determine the relative basal-to-apical distributions of WT and modified VSV G and GP64 constructs, individual cells were assessed for the mean gray values of protein staining in a rectangular region of interest (ROI) adjusted to the width of each cell along the basal-to-apical axis of the cell. The polarized orientations of midgut or salivary gland cells were identified by the positions of phalloidin-stained actin in the basal visceral muscles and the apical brush border, and by differential interference contrast (DIC) microscopy. In some instances, when midgut cells were slightly curved, a segmented (curved) ROI was selected to account for the cell curvature. The same ROI was used to measure the mean gray values of the immunostained VSV G or GP64 (Alexa 647) and nuclear (DAPI) signals. The images were derived from discrete focal planes and we evaluated only the cells with a nucleus that clearly bisected the cell, to ensure that localization data encompassed the basal to apical limits of each individual cell. In addition, we assessed large numbers of cells ($n \geq 69$ per genotype) from tissues derived from at least 3 individual animals in triplicate experiments.

Because we found that VSV $G^{\Delta Y}$ and $GP64^{\Delta Y}$ proteins were present at lower levels than those of the corresponding WT proteins (e.g. Fig. S6), we measured the differences in the cellular distributions of WT vs. ΔY constructs for these studies. Because cells were not uniform in size or staining intensity, the basal-to-apical distance was expressed in percentage values, and the signal (VSV G, GP64, and DAPI) intensity within each cell was standardized based on the average signal intensity within that cell. The resulting standardized gray values of each cell were binned in 5% intervals across the basal-to-apical axis (to account for differences in cell sizes), averaged across all cells for each condition, and plotted onto graphs. The percentage of total viral protein signal in

the apical (top 40%) and basolateral (bottom 20%) compartments of enterocytes and salivary gland cells were quantified from these data to determine the effects of the tyrosine motif mutation and various RNAi of host trafficking components on viral protein distribution in these compartments. These compartments in enterocytes were selected based on DLG and DAPI staining to represent areas of the apical and basolateral compartments relatively free from any interference of the nucleus where the viral protein is absent (Fig. S1). Distinguishing between the apical and basolateral compartments in *Drosophila* salivary gland cells is difficult due to their unique structure [*i.e.*, extensive apical membrane invaginations (canaliculi) reaching deep inside the cell (Fig. 1C)], and therefore could not be accurately determined with our current method. Since these invaginations rarely extend past the nuclei, as indicated by phalloidin staining of the actin-rich canaliculi (Fig. S2C), we decided to quantify viral protein signal in the bottom (basal) 20% of the salivary gland cells to minimize any influence of the nucleus or canaliculi (Fig. S1). The master gain of the laser for acquiring VSV G or GP64 and nuclear stain signals was optimized for each image to avoid pixel saturation. Data shown was compiled from 3 independent experiments, in which ≥ 20 cells from at least 3 individual midguts or salivary glands (total n ≥ 69) were assessed per experiment. The total number of cells used for each quantification is noted in the figure legends.

We measured and compared the basal-to-apical distributions of each of the WT vs. ΔY constructs. To assess the total levels of VSV G^{WT} and VSV $G^{\Delta Y}$ staining in cells, the Integrated Density values (IntDen = Mean Gray × Area) were determined in ROIs drawn around entire cells (guided by actin staining and/or DIC images) using the freehand tool in ImageJ. The master gain of the laser for acquiring VSV G stain signals was kept constant (while avoiding pixel saturation) for all samples. The numbers of cells used for each quantification of total VSV G levels in enterocytes were: VSV G^{WT} (n = 44), VSV $G^{\Delta Y}$ (n = 40), Negative (N) (n = 53).

Statistical analysis

The viral protein signal in the apical (top 40%) and basolateral (bottom 20%) compartments of enterocytes and salivary gland cells were assessed statistically for differences relative to controls (WT protein or samples lacking RNAi) upon tyrosine motif mutation and various RNAi targeting host trafficking components. All statistical analyses were conducted using R Statistical Software (RStudio v.4.1.2) (80). Data for each condition was subjected to the Shapiro–Wilk test to

768 determine whether it was normally distributed. For single comparisons of conditions, Welch's t-
769 test was used to compare normally distributed data, while the Wilcoxon rank-sum test was used to
770 compare data that were not normally distributed. For multiple comparisons of conditions, one-way
771 analysis of variance (ANOVA) was used to compare normally distributed data, while the Kruskal–
772 Wallis test was used to compare data that were not normally distributed. If statistically significant
773 differences overall were found ($p \leq 0.05$), then a *post hoc* multiple comparison analysis (with
774 Bonferroni p-value correction) was performed to identify which specific conditions were
775 significantly different from each other.
776
777 **Data Availability**
778 All data are available in the article and supplemental material.
779
780

781 **Acknowledgements**
782 The authors thank F. M. Boyce (Massachusetts General Hospital) for providing plasmid VSVG-
783 BP95NOTSV, Gary Whittaker (Cornell University) for providing anti-VSV G antibody 8G5F11,
784 Mikio Furuse (National Institute for Physiological Sciences, Japan) for antibodies directed against
785 Snakeskin and Tetraspanin 2A, and Bruce Edgar (University of Utah) for E-Cadherin-GFP
786 *Drosophila* line. We also thank Peter Nagy for assistance and expertise with initial Rab GTPase
787 localization mapping.
788
789

790 **Author Contributions**
791 Conceptualization: Nicolas Buchon, Gary Blissard, Jeffrey Hodgson.
792 Formal analysis: Jeffrey Hodgson, Robin Chen, Nicolas Buchon, Gary Blissard
793 Funding acquisition: Gary Blissard, Nicolas Buchon.
794 Investigation: Jeffrey Hodgson, Robin Chen, Nicolas Buchon, Gary Blissard.
795 Methodology: Jeffrey Hodgson, Robin Chen, Nicolas Buchon, Gary Blissard.
796 Project administration: Gary Blissard, Nicolas Buchon.
797 Supervision: Nicolas Buchon, Gary Blissard.

Writing – original draft: Jeffrey Hodgson, Robin Chen.

Writing – review & editing: Jeffrey Hodgson, Robin Chen, Gary Blissard, Nicolas Buchon.

References

1. Moscardi F. 1999. Assessment of the application of baculoviruses for control of Lepidoptera. Annu Rev Entomol 44:257-89.PMID: 15012374
2. Possee RD, King LA. 2014. Insect Viruses, eLS doi:10.1002/9780470015902.a0020712.pub2.
3. Rohrmann GF. 2019. Baculoviruses as insecticides: Four examples in Baculovirus Molecular Biology, 4th ed: Chapter 9 (ebook). National Center for Biotechnology Information (US), Bethesda (MD).
4. Fact-Sheet. 2024. Vector-borne diseases, *on* World Health Organization. https://www.who.int/news-room/fact-sheets/detail/vector-borne-diseases. Accessed Jan. 18, 2024.
5. Pereira Cabral B, da Graca Derengowski Fonseca M, Mota FB. 2019. Long term prevention and vector control of arboviral diseases: What does the future hold? Int J Infect Dis 89:169-174.PMID: 31606414
6. Kading RC, Brault AC, Beckham JD. 2020. Global Perspectives on Arbovirus Outbreaks: A 2020 Snapshot. Trop Med Infect Dis 5.PMID: 32906771
7. Ma E, Zhu Y, Liu Z, Wei T, Wang P, Cheng G. 2021. Interaction of Viruses with the Insect Intestine. Annu Rev Virol 8:115-131.PMID: 33872516
8. Buchon N, Osman D. 2015. All for one and one for all: Regionalization of the *Drosophila* intestine. Insect Biochem Mol Biol 67:2-8.PMID: 26044368
9. Girdler GC, Roper K. 2014. Controlling cell shape changes during salivary gland tube formation in Drosophila. Semin Cell Dev Biol 31:74-81.PMID: 24685610
10. Buchon N, Osman D, David FP, Yu Fang H, Boquete JP, Deplancke B, Lemaitre B. 2013. Morphological and molecular characterization of adult midgut compartmentalization in *Drosophila*. Cell Rep 3:1725-38.PMID: 23643535
11. Bonfini A, Liu X, Buchon N. 2016. From pathogens to microbiota: How Drosophila intestinal stem cells react to gut microbes. Dev Comp Immunol 64:22-38.PMID: 26855015
12. Liu X, Nagy P, Bonfini A, Houtz P, Bing XL, Yang X, Buchon N. 2022. Microbes affect gut epithelial cell composition through immune-dependent regulation of intestinal stem cell differentiation. Cell Rep 38:110572.PMID: 35354023
13. Miguel-Aliaga I, Jasper H, Lemaitre B. 2018. Anatomy and Physiology of the Digestive Tract of Drosophila melanogaster. Genetics 210:357-396.PMID: 30287514
14. Rivera-Vega LJ, Acevedo FE, Felton GW. 2017. Genomics of Lepidoptera saliva reveals function in herbivory. Curr Opin Insect Sci 19:61-69.PMID: 28521944
15. Ribeiro JM, Francischetti IM. 2003. Role of arthropod saliva in blood feeding: sialome and post-sialome perspectives. Annu Rev Entomol 48:73-88.PMID: 12194906
16. Walker GP. 2009. Chapter 228 - Salivary Glands, p 897-901. *In* Resh VH, Cardé RT (ed), Encyclopedia of Insects (Second Edition) doi:https://doi.org/10.1016/B978-0-12-374144-8.00237-X. Academic Press, San Diego.
17. Van Ree C. 2021. The adult Drosophila salivary gland: developing a new epithelial research model. MS. University of Melbourne.

18. Döhner K, Sodeik B. 2005. The Role of the Cytoskeleton During Viral Infection, p 67-108. *In* Marsh M (ed), Membrane Trafficking in Viral Replication doi:10.1007/3-540-26764-6_3. Springer Berlin Heidelberg, Berlin, Heidelberg.
19. Hsu NY, Ilnytska O, Belov G, Santiana M, Chen YH, Takvorian PM, Pau C, van der Schaar H, Kaushik-Basu N, Balla T, Cameron CE, Ehrenfeld E, van Kuppeveld FJ, Altan-Bonnet N. 2010. Viral reorganization of the secretory pathway generates distinct organelles for RNA replication. Cell 141:799-811.PMID: 20510927
20. Zeltzer S, Zeltzer Carol A, Igarashi S, Wilson J, Donaldson Julie G, Goodrum F. 2018. Virus Control of Trafficking from Sorting Endosomes. mBio 9:10.1128/mbio.00683-18.PMID:
21. Tognarelli EI, Reyes A, Corrales N, Carreño LJ, Bueno SM, Kalergis AM, González PA. 2021. Modulation of Endosome Function, Vesicle Trafficking and Autophagy by Human Herpesviruses. Cells. 10(3):doi:10.3390/cells10030542.
22. Sobhy H. 2016. A Review of Functional Motifs Utilized by Viruses. Proteomes 4.PMID: 28248213
23. Mihalič F, Simonetti L, Giudice G, Sander MR, Lindqvist R, Peters MBA, Benz C, Kassa E, Badgujar D, Inturi R, Ali M, Krystkowiak I, Sayadi A, Andersson E, Aronsson H, Söderberg O, Dobritzsch D, Petsalaki E, Överby AK, Jemth P, Davey NE, Ivarsson Y. 2023. Large-scale phage-based screening reveals extensive pan-viral mimicry of host short linear motifs. Nature Communications 14:2409.PMID:
24. Popham HJ, Nusawardani T, Bonning BC. 2016. Introduction to the Use of Baculoviruses as Biological Insecticides. Methods Mol Biol 1350:383-392.PMID: 26820869
25. USDA-APHIS. May 2023. Vesicular Stomatitis Fact Sheet. USDA, U.S. Department of Agriculture Animal and Plant Health Inspection Service, APHIS.USDA.gov. https://www.aphis.usda.gov/aphis/ourfocus/animalhealth/animal-disease-information/equine/vsv/vesicular-stomatitis.
26. Blissard GW, Theilmann DA. 2018. Baculovirus entry and egress from insect cells. Annu Rev Virol 5:113-139.PMID: 30004832
27. Albertini AA, Baquero E, Ferlin A, Gaudin Y. 2012. Molecular and cellular aspects of rhabdovirus entry. Viruses 4:117-39.PMID: 22355455
28. Sevier CS, Weisz OA, Davis M, Machamer CE. 2000. Efficient Export of the Vesicular Stomatitis Virus G Protein from the Endoplasmic Reticulum Requires a Signal in the Cytoplasmic Tail That Includes Both Tyrosine-based and Di-acidic Motifs. Mol Biol Cell 11:13-22.PMID: 10637287
29. Thomas DC, Roth MG. 1994. The basolateral targeting signal in the cytoplasmic domain of glycoprotein G from vesicular stomatitis virus resembles a variety of intracellular targeting motifs related by primary sequence but having diverse targeting activities. J Biol Chem 269:15732-9.PMID: 8195226
30. Thomas DC, Brewer CB, Roth MG. 1993. Vesicular stomatitis virus glycoprotein contains a dominant cytoplasmic basolateral sorting signal critically dependent upon a tyrosine. J Biol Chem 268:3313-20.PMID:
31. Hodgson JJ, Buchon N, Blissard GW. 2022. Identification of cellular genes involved in baculovirus GP64 trafficking to the plasma membrane. Journal of Virology 96:e0021522.PMID: 35608346

32. Dong S, Blissard GW. 2012. Functional analysis of the *Autographa californica* multiple nucleopolyhedrovirus GP64 terminal fusion loops and interactions with membranes. J Virol 86:9617-9628.PMID: 22740400
33. Keddie BA, Aponte GW, Volkman LE. 1989. The pathway of infection of *Autographa californica* nuclear polyhedrosis virus in an insect host. Science 243:1728-1730.PMID: 2648574
34. Lucas W. 2010. Viral Capsids and Envelopes: Structure and Function, Encyclopedia of Life Sciences doi:10.1002/9780470015902.a0001091.pub2.
35. Navaratnarajah CK, Warrier R, Kuhn RJ. 2008. Assembly of Viruses: Enveloped Particles, p 193-200. *In* Mahy BWJ, Van Regenmortel MHV (ed), Encyclopedia of Virology (Third Edition) doi:https://doi.org/10.1016/B978-012374410-4.00667-1. Academic Press, Oxford.
36. Clem RJ, Passarelli AL. 2013. Baculoviruses: sophisticated pathogens of insects. PLoS Pathog 9:e1003729.PMID: 24244160
37. Dietzgen RG, Kuzmin IV. 2012. Rhabdoviruses: Molecular Taxonomy, Evolution, Genomics, Ecology, Host-vector Interactions, Cytopathology and Control. Caister Academic Press.
38. Stalder D, Gershlick DC. 2020. Direct trafficking pathways from the Golgi apparatus to the plasma membrane. Semin Cell Dev Biol 107:112-125.PMID: 32317144
39. Lippincott-Schwartz J, Roberts TH, Hirschberg K. 2000. Secretory protein trafficking and organelle dynamics in living cells. Annu Rev Cell Dev Biol 16:557-89.PMID: 11031247
40. Xiang Y, Zhang X, Nix DB, Katoh T, Aoki K, Tiemeyer M, Wang Y. 2013. Regulation of protein glycosylation and sorting by the Golgi matrix proteins GRASP55/65. Nat Commun 4:1659.PMID: 23552074
41. Franz AW, Kantor AM, Passarelli AL, Clem RJ. 2015. Tissue Barriers to Arbovirus Infection in Mosquitoes. Viruses 7:3741-3767.PMID: 26184281
42. Sanchez-Vargas I, Olson KE, Black WCt. 2021. The Genetic Basis for Salivary Gland Barriers to Arboviral Transmission. Insects 12.PMID: 33467430
43. Palmer WH, Dittmar M, Gordesky-Gold B, Hofmann J, Cherry S. 2020. Drosophila melanogaster as a model for arbovirus infection of adult salivary glands. Virology 543:1-6.PMID: 32056841
44. Wells MB, Villamor J, Andrew DJ. 2017. Salivary gland maturation and duct formation in the African malaria mosquito Anopheles gambiae. Sci Rep 7:601.PMID: 28377572
45. Wells MB, Andrew DJ. 2015. Salivary gland cellular architecture in the Asian malaria vector mosquito Anopheles stephensi. Parasit Vectors 8:617.PMID: 26627194
46. Hung RJ, Hu Y, Kirchner R, Liu Y, Xu C, Comjean A, Tattikota SG, Li F, Song W, Ho Sui S, Perrimon N. 2020. A cell atlas of the adult Drosophila midgut. Proc Natl Acad Sci U S A 117:1514-1523.PMID: 31915294
47. Shanbhag S, Tripathi S. 2009. Epithelial ultrastructure and cellular mechanisms of acid and base transport in the Drosophila midgut. J Exp Biol 212:1731-44.PMID: 19448082
48. Backovic M, Jardetzky TS. 2011. Class III viral membrane fusion proteins. Adv Exp Med Biol 714:91-101.PMID: 21506008
49. Yuan S, Chu H, Huang J, Zhao X, Ye ZW, Lai PM, Wen L, Cai JP, Mo Y, Cao J, Liang R, Poon VK, Sze KH, Zhou J, To KK, Chen Z, Chen H, Jin DY, Chan JF, Yuen KY. 2020. Viruses

harness YxxØ motif to interact with host AP2M1 for replication: A vulnerable broad-spectrum antiviral target. Sci Adv 6:eaba7910.PMID: 32923629
50. Stenmark H. 2009. Rab GTPases as coordinators of vesicle traffic. Nat Rev Mol Cell Biol 10:513-25.PMID: 19603039
51. Chua CEL, Tang BL. 2018. Rab 10-a traffic controller in multiple cellular pathways and locations. J Cell Physiol 233:6483-6494.PMID: 29377137
52. Henry L, Sheff DR. 2008. Rab8 regulates basolateral secretory, but not recycling, traffic at the recycling endosome. Mol Biol Cell 19:2059-68.PMID: 18287531
53. Ang AL, Folsch H, Koivisto UM, Pypaert M, Mellman I. 2003. The Rab8 GTPase selectively regulates AP-1B-dependent basolateral transport in polarized Madin-Darby canine kidney cells. J Cell Biol 163:339-50.PMID: 14581456
54. Bu Y, Teng Q, Feng D, Sun L, Xue J, Zhang G. 2021. YLMY Tyrosine Residue within the Cytoplasmic Tail of Newcastle Disease Virus Fusion Protein Regulates Its Surface Expression to Modulate Viral Budding and Pathogenicity. Microbiol Spectr 9:e0217321.PMID: 34937182
55. Gunner P. Johnston EMC, Jeffrey Dabundo, Bryce A. Henderson, Keesha M. Matz, Victoria Ortega, Alfredo Ramirez, Arnold Park, Hector C. Aguilara. 2017. Cytoplasmic Motifs in the Nipah Virus Fusion Protein Modulate Virus Particle Assembly and Egress. J Virol doi:10.1128/JVI.02150-16.PMID:
56. Devergne O, Sun GH, Schupbach T. 2017. Stratum, a Homolog of the Human GEF Mss4, Partnered with Rab8, Controls the Basal Restriction of Basement Membrane Proteins in Epithelial Cells. Cell Rep 18:1831-1839.PMID: 28228250
57. Lerner DW, McCoy D, Isabella AJ, Mahowald AP, Gerlach GF, Chaudhry TA, Horne-Badovinac S. 2013. A Rab10-dependent mechanism for polarized basement membrane secretion during organ morphogenesis. Dev Cell 24:159-68.PMID: 23369713
58. Zajac AL, Horne-Badovinac S. 2022. Kinesin-directed secretion of basement membrane proteins to a subdomain of the basolateral surface in Drosophila epithelial cells. Curr Biol 32:735-748 e10.PMID: 35021047
59. Parker SS, Cox C, Wilson JM. 2018. Rabs set the stage for polarity. Small GTPases 9:116-129.PMID: 28125340
60. Gui J, Huang Y, Shimmi O. 2016. Scribbled Optimizes BMP Signaling through Its Receptor Internalization to the Rab5 Endosome and Promote Robust Epithelial Morphogenesis. PLoS Genet 12:e1006424.PMID: 27814354
61. Wilson B, Flett C, Gemperle J, Lawless C, Hartshorn M, Hinde E, Harrison T, Chastney M, Taylor S, Allen J, Norman JC, Zacharchenko T, Caswell PT. 2023. Proximity labelling identifies pro-migratory endocytic recycling cargo and machinery of the Rab4 and Rab11 families. J Cell Sci 136.PMID: 37232246
62. Zhang J, Schulze KL, Hiesinger PR, Suyama K, Wang S, Fish M, Acar M, Hoskins RA, Bellen HJ, Scott MP. 2007. Thirty-one flavors of *Drosophila* Rab proteins. Genetics 176:1307-22.PMID: 17409086
63. Vega-Rúa A, Schmitt C, Bonne I, Krijnse Locker J, Failloux AB. 2015. Chikungunya Virus Replication in Salivary Glands of the Mosquito Aedes albopictus. Viruses 7:5902-7.PMID: 26593936
64. Oschman JL, Berridge MJ. 1970. Structural and functional aspects of salivary fluid section in Calliphora. Tissue Cell 2:281-310.PMID: 18631514

65. Park SY, Guo X. 2014. Adaptor protein complexes and intracellular transport. Biosci Rep 34.PMID: 24975939
66. Ohno H, Stewart J, Fournier M-C, Bosshart H, Rhee I, Miyatake S, Saito T, Gallusser A, Kirchhausen T, Bonifacino Juan S. 1995. Interaction of Tyrosine-Based Sorting Signals with Clathrin-Associated Proteins. Science 269:1872-1875.PMID:
67. Bonifacino JS. 2014. Adaptor proteins involved in polarized sorting. J Cell Biol 204:7-17.PMID: 24395635
68. Mardones GA, Burgos PV, Lin Y, Kloer DP, Magadan JG, Hurley JH, Bonifacino JS. 2013. Structural basis for the recognition of tyrosine-based sorting signals by the mu3A subunit of the AP-3 adaptor complex. J Biol Chem 288:9563-71.PMID: 23404500
69. Guo X, Mattera R, Ren X, Chen Y, Retamal C, González A, Bonifacino Juan S. 2013. The Adaptor Protein-1 μ1B Subunit Expands the Repertoire of Basolateral Sorting Signal Recognition in Epithelial Cells. Developmental Cell 27:353-366.PMID:
70. Sosa RT, Weber MM, Wen Y, O'Halloran TJ. 2012. A single beta adaptin contributes to AP1 and AP2 complexes and clathrin function in Dictyostelium. Traffic 13:305-16.PMID: 22050483
71. Folsch H. 2015. Analyzing the role of AP-1B in polarized sorting from recycling endosomes in epithelial cells. Methods Cell Biol 130:289-305.PMID: 26360041
72. Blumstein J, Faundez V, Nakatsu F, Saito T, Ohno H, Kelly RB. 2001. The neuronal form of adaptor protein-3 is required for synaptic vesicle formation from endosomes. J Neurosci 21:8034-42.PMID: 11588176
73. Olson JK, Grose C. 1997. Endocytosis and recycling of varicella-zoster virus Fc receptor glycoprotein gE: internalization mediated by a YXXL motif in the cytoplasmic tail. J Virol 71:4042-54.PMID: 9094682
74. Heineman TC, Hall SL. 2001. VZV gB endocytosis and Golgi localization are mediated by YXXphi motifs in its cytoplasmic domain. Virology 285:42-9.PMID: 11414804
75. Li Y, Marzolo MP, van Kerkhof P, Strous GJ, Bu G. 2000. The YXXL motif, but not the two NPXY motifs, serves as the dominant endocytosis signal for low density lipoprotein receptor-related protein. J Biol Chem 275:17187-94.PMID: 10747918
76. Ang SF, Folsch H. 2012. The role of secretory and endocytic pathways in the maintenance of cell polarity. Essays Biochem 53:29-39.PMID: 22928506
77. Ang AL, Taguchi T, Francis S, Folsch H, Murrells LJ, Pypaert M, Warren G, Mellman I. 2004. Recycling endosomes can serve as intermediates during transport from the Golgi to the plasma membrane of MDCK cells. The Journal of cell biology 167:531-43.PMID: 15534004
78. Grant BD, Donaldson JG. 2009. Pathways and mechanisms of endocytic recycling. Nat Rev Mol Cell Biol 10:597-608.PMID: 19696797
79. Yu S, Nie Y, Knowles B, Sakamori R, Stypulkowski E, Patel C, Das S, Douard V, Ferraris RP, Bonder EM, Goldenring JR, Ip YT, Gao N. 2014. TLR sorting by Rab11 endosomes maintains intestinal epithelial-microbial homeostasis. Embo j 33:1882-95.PMID: 25063677
80. Team RC. 2023. R: A language and environment for statistical computing, *on* R Foundation for Statistical Computing. https://www.R-project.org/. Accessed 2023.

Figure Legends

Figure 1.

Localization of VSV G and GP64 in *Drosophila* midgut and salivary gland cells in the absence of VSV or baculovirus infection. **(A)** Schematic representation of a *Drosophila* midgut enterocyte illustrating the polarized morphology with apical microvilli (red, top) adjacent to the gut lumen, and basal membrane (gray) adjacent to the visceral muscles (red, bottom). The relative locations of the nuclei (blue) and polarity marker proteins for septate junctions (Discs large; magenta) and adherens junctions (E-Cadherin; gold) are indicated. **(B)** Localization of VSV G (top panels) and GP64 (bottom panels) ectopically expressed in adult *Drosophila* midgut tissue (left) and individual enterocytes (dashed box, right). **(C)** Schematic representation of an adult *Drosophila* salivary gland epithelial cell showing deep invaginations of the apical membrane (canaliculi; red). The relative location of the nucleus (blue) and polarity marker proteins for septate junctions (Discs large; magenta) and adherens junctions (E-Cadherin; gold) are indicated. **(D)** Localization of VSV G (top panels) and GP64 (bottom panels) in adult *Drosophila* salivary gland tissue (left) and individual salivary gland epithelial cells (dashed box, right). Tissues were dissected from adult *Drosophila* expressing each viral envelope protein ubiquitously under the *da-GAL4, tub-GAL80^{ts}* driver. At 3 to 7 days post-eclosion, flies developed at 18º C were shifted to 29º C for 3 days to induce expression of VSV G or GP64. Viral envelope proteins (green) were labelled with mouse anti-VSV G or anti-GP64 primary antibodies and Alexa Fluor 647 donkey anti-mouse secondary antibody, actin (red) was labelled with Alexa Fluor 555 phalloidin, and nuclei (blue) were stained with DAPI. Scale bars are 25 μm for tissue images (left) and 5 μm (midgut) or 10 μm (salivary gland) for cellular images (right).

Figure 2.

Analysis of the role(s) of VSV G and GP64 cytoplasmic YxxØ motifs for envelope protein trafficking in *Drosophila* midgut enterocytes and salivary gland cells. **(A)** Schematic illustrating the transmembrane (TM) and cytoplasmic tail domains of VSV G and GP64, and illustrating the locations of the YxxØ motif (yellow highlight) in each protein and the engineered alanine substitutions (lower case "a"). **(B)** Representative images showing the distribution of WT (left) and alanine-substituted (right, ΔY) viral envelope proteins (VSV G and GP64) in midgut enterocytes after 3 days of ubiquitous expression under the *da-GAL4, tub-GAL80^{ts}* driver. A graph

comparing the average relative distributions (basal-to-apical) of each protein (WT vs. ΔY) is shown on the right of each pair of immunofluroescence images. The average relative position of the nucleus (determined by DAPI signal intensity) was plotted as a light gray line in the background of each graph to indicate areas relatively free from its influence (shaded gray areas). The basal and apical regions on the graphs were established based on the location of the septate junctions (discs-large polarity marker) (Fig. S1), and the division is indicated at approximately 52.5% on the x-axis by a vertical dashed line. **(C)** Representative images show the distribution of WT (left) and modified (right, ΔY) viral envelope proteins (VSV G and GP64) in salivary gland cells. As above, a graph comparing the average relative distributions (basal-to-apical) of each protein (WT vs. ΔY) is shown on the right of each pair of immunofluorescence images. The average relative position of the nucleus was also plotted as a gray line. The average cell height (basal-to-apical distance in %) (x-axis) and signal intensities (y-axis) were measured and calculated as described in the Materials and Methods section. The shaded areas on each graph represent the areas of the cell (basal 20% and apical 40%) relatively free from influence of the nuclei used for statistical analyses. Number of asterisks refer to the level of statistical significance (n.s. $p > 0.05$, * $p \leq 0.05$, ** $p \leq 0.01$, *** $p \leq 0.001$, and **** $p \leq 0.0001$) between distributions of WT and alanine-substituted (ΔY) envelope proteins in the shaded areas. The numbers of midgut enterocytes used to generate the graphs were: VSV G^{WT} n = 69; VSV $G^{\Delta Y}$ n = 96; $GP64^{WT}$ n = 90; $GP64^{\Delta Y}$ n = 106. The numbers of salivary gland cells used to generate the graphs were: VSV G^{WT} n = 160; VSV $G^{\Delta Y}$ n = 211; $GP64^{WT}$ n = 163; $GP64^{\Delta Y}$ n = 186. Data shown represents combined results from 3 independent experiments. Viral envelope proteins (white) were labelled with mouse anti-VSV G or anti-GP64 primary antibodies and Alexa Fluor 647 donkey anti-mouse secondary antibody. Scale bars represent 5 μm.

Figure 3.

Effects of RNAi of clathrin adaptor protein subunits on basal trafficking of VSV G in *Drosophila* midgut enterocytes. The image panels (left) show the localization of VSV G (green in images on the left and white in images on the right) in enterocytes from either control flies (top row, no RNAi) or from flies co-expressing VSV G and RNAi constructs to deplete AP-1μ, AP-2μ, AP-3μ, or AP-1,2β (indicated on the left of each row). The graph in each row compares the basal-to-apical distribution of VSV G in control enterocytes (top panels) against enterocytes from flies co-expressing VSV G and an RNAi construct (indicated on the left of each row of image panels). For all RNAi flies, distribution of VSV G was analyzed after 3 days of RNAi induction under the midgut *Myo-GAL4, tub-GAL80^{ts}* driver. The average relative position of the nucleus was also plotted as a gray line. The average cell height (basal-to-apical distance in %) (x-axis) and VSV G signal intensities (y-axis) were measured and calculated as described in the Materials and Methods section. The basal and apical regions on the graphs were established based on the location of the septate junction (discs-large polarity marker) (Fig. S1), and the division is indicated at 52.5% on the x-axis by a vertical dashed line. The shaded areas on each graph represent the areas of the cell (basal 20% and apical 40%) relatively free from influence of the nuclei and used for statistical analyses. The number of asterisks in the shaded areas refer to the level of statistical significance (n.s. $p > 0.05$, * $p \leq 0.05$, ** $p \leq 0.01$, *** $p \leq 0.001$, and **** $p \leq 0.0001$) in VSV G distribution differences between RNAi and control flies in those areas. The numbers of midgut enterocytes analyzed were: Control (n = 165), AP-1μ RNAi (n = 141), AP-2μ RNAi (n = 119), AP-3μ RNAi (n = 122), and AP-1,2β RNAi (n = 146). Data shown represents combined results from 3 independent experiments. Viral envelope protein (green) was labelled with mouse anti-VSV G primary antibody and Alexa Fluor 647 donkey anti-mouse secondary antibody, actin (red) was labelled with Alexa Fluor 555 phalloidin, and nuclei (blue) were stained with DAPI. Scale bars represent 5 μm.

Figure 4

Rab GTPase localization patterns in *Drosophila* midgut enterocytes and salivary gland cells illustrated by representative images of immunostained YFP-tagged Rab GTPases (green). The YFP-tagged Rab GTPases were expressed ubiquitously in adult *Drosophila* under the *da-GAL4,*

tub-GAL80^{ts} driver for 3 days before dissection and immunostaining with chicken anti-GFP primary antibody and Alexa Fluor 488 goat anti-chicken secondary antibody (green). Actin (red) was labelled with Alexa Fluor 555 phalloidin, nuclei (blue) were stained with DAPI, and Discs large (magenta) was stained with mouse anti-Discs large primary antibody and Alexa Fluor 647 donkey anti-mouse secondary antibody. Scale bars represent 5 μm.

Figure 5.

Effects of RNAi of selected Rab GTPases on basal trafficking of VSV G in *Drosophila* midgut enterocytes. The image panels (left) show the localization of VSV G (green in images on the left and white in images on the right) in enterocytes from either control flies (top row, no RNAi) or from flies co-expressing VSV G and RNAi constructs to deplete Rab1, Rab4, Rab8, Rab10, Rab11, Rab23, Rab30, or Rab35 (indicated on the left of each row of image panels). For all RNAi flies (except Rab11), distribution of VSV G was analyzed after 5 days of RNAi induction (3 days for Rab11) under the midgut *Myo-GAL4, tub-GAL80^{ts}* driver. The average relative position of the nucleus was also plotted as a gray line. The average cell height (basal-to-apical distance in %) (x-axis) and VSV G signal intensities (y-axis) were measured and calculated as described in the Materials and Methods section. The basal and apical regions on the graphs were established based on the location of the septate junction (discs-large polarity marker) (Fig. S1), and the division is indicated at 52.5% on the x-axis by a vertical dashed line. The shaded areas on each graph represent the areas of the cell (basal 20% and apical 40%) relatively free from influence of the nuclei and used for statistical analyses. The number of asterisks in the shaded areas of the graphs refer to the level of statistical significance (n.s. $p > 0.05$, * $p \leq 0.05$, ** $p \leq 0.01$, *** $p \leq 0.001$, and **** $p \leq 0.0001$) in VSV G distribution between RNAi and control flies. The numbers of midgut enterocytes analyzed were: Control (n = 572), Rab1 RNAi (n = 140), Rab4 RNAi (n = 150), Rab8 RNAi (n = 138), Rab10 RNAi (n = 124), Rab11 (n = 131), Rab23 RNAi (n = 210), Rab30 RNAi (n = 207), Rab35 RNAi (n = 235). Data shown represent combined results from 3 independent experiments with each RNAi compared to its appropriate control. Viral envelope protein (green) was labelled with mouse anti-VSV G primary antibody and Alexa Fluor 647 donkey anti-mouse secondary antibody, actin (red) was labelled with Alexa Fluor 555 phalloidin, and nuclei (blue) were stained with DAPI. Scale bars represent 5 μm.

1137 **----------**

1138 **Supplemental Data**

1139 **Figure S1.**

1140 The method for quantifying relative viral envelope protein distribution along the basal-to-apical
1141 axis in *Drosophila* midgut enterocytes and salivary gland cells. **(A)** Regions of interest (ROI,
1142 shown in yellow) from which signal intensity was measured along the basal-to-apical axis using
1143 ImageJ (as described in the Materials and Methods section). **(B)** Distribution of select marker
1144 proteins in midgut enterocytes and salivary gland cells. The peak in Discs large signal in
1145 enterocytes at the 52.5% mark (vertical dashed line) represents the location of septate junctions
1146 that define the boundaries between the basal and apical compartments. Phalloidin staining was
1147 used to assess the distribution of cortical actin in the salivary gland cells, indicative of the apical
1148 membrane invaginations. Phalloidin staining pattern and signal distribution closely approximate
1149 VSV G signal distribution (Fig. 2C and S2C), suggesting co-localization. The average signal
1150 distribution density is indicated by the horizontal dashed line and data points above the horizontal
1151 dashed line show regions of marker protein enrichment. **(C)** Locations of midgut enterocyte and
1152 salivary gland cell nuclei were determined by DAPI (blue line) signal distribution. The regions
1153 selected for statistical analysis to detect changes in viral envelope protein distribution are indicated
1154 by gray boxes. Those regions were selected based on average locations of marker proteins and
1155 nuclei (see the Materials and Methods section for details).
1156
1157
1158 **Figure S2.**
1159 Cellular structural marker proteins in *Drosophila* midgut enterocytes and salivary gland epithelial
1160 cells. Tissues from flies constitutively expressing GFP-tagged E-Cadherin (labelling adherens
1161 junctions) were dissected, fixed and immunostained for Discs large (labelling septate junctions),
1162 Snakeskin (labelling septate junctions), Integrin β1 (labelling basal membrane), Tetraspannin 2A
1163 (labelling septate junctions), phalloidin (labeling cortical actin and visceral muscles), and DAPI
1164 (labeling DNA in nuclei). Scale bars represent 5 μm.
1165
1166 **Figure S3.**

Localization patterns of VSV G in *Drosophila* salivary gland cells are variable. On the left, a bar graph illustrates the proportion of salivary gland cells displaying either basal, non-polarized, or apical enrichment patterns of VSV G^{WT} (n = 160) and VSV $G^{\Delta Y}$ (n = 211). Basal enrichment was found in 18.8% and 4.27% of salivary gland cells expressing VSV G^{WT} and VSV $G^{\Delta Y}$, respectively. Non-polar distribution pattern was found in 52.5% and 54.5% of salivary gland cells expressing VSV G^{WT} and VSV $G^{\Delta Y}$, respectively. Apical distribution pattern was found in 28.8% and 41.2% of salivary gland cells expressing VSV G^{WT} and VSV $G^{\Delta Y}$, respectively. Immunofluorescence images on the right illustrate examples of each pattern of VSV G localization. A vast majority of the salivary gland cells (81.3% for VSV G^{WT} and 95.7% for VSV $G^{\Delta Y}$) showed presence of VSV G in apical regions. We found that the proportion of salivary gland cells with apically localized VSV $G^{\Delta Y}$ (95.7%, n = 211) was slightly increased compared to cells expressing VSV G^{WT} (81.3%, n = 160) (Chi-squared test: $\chi^2 = 18.8$, df = 1, $p = 1.46 \times 10^{-5}$). Also, the proportion of cells with basally localized VSV $G^{\Delta Y}$ was slightly decreased in comparison to VSV G^{WT} (13.8 ± 0.56% for VSV $G^{\Delta Y}$ vs. 23.4 ± 0.97% for VSV G^{WT}, w = 25056, $p = 1.33 \times 10^{-15}$). VSV G was labelled with mouse anti-VSV G primary antibody and Alexa Fluor 647 donkey anti-mouse secondary antibody and nuclei were stained with DAPI. Scale bars represent 5 μm.

Figure S4.

Anthranilic acid inhibits basal VSV G trafficking in *Drosophila* midgut enterocytes. At 3-5 days post-eclosion, flies carrying an inducible VSV G expression construct (*Myo-GAL4, UAS-nlsGFP, tub-GAL80^{ts}; UAS-VSV G^{WT}*) were exposed to anthranilic acid-treated artificial diet (ACA; 240 mg dissolved in 300 μL of 100% ethanol applied onto the surface of ~10 mL of artificial diet) or the ethanol vehicle-treated diet (ETH; 300 μL of 100% ethanol) for 3 days at 18°C before shifting to 29°C for 48 h to induce VSV G expression. The average relative position of the nucleus was also plotted as a gray line. The average cell height (basal-to-apical distance in %) (x-axis) and signal intensities (y-axis) were measured and calculated as described in the Materials and Methods section. The basal-to-apical distribution of VSV G resulting from each treatment is shown on the graph. The basal and apical regions on the graphs were established based on the location of the septate junction (discs-large polarity marker) (Fig. S1), and the division is indicated at 52.5% on the x-axis by a vertical dashed line. The shaded areas on each graph represent the areas of the cell

(basal 20% and apical 40%) relatively free from influence of the nuclei and used for statistical analyses. The number of asterisks refer to the level of statistical significance (n.s. $p > 0.05$, * $p \leq 0.05$, ** $p \leq 0.01$, *** $p \leq 0.001$, and **** $p \leq 0.0001$) between distributions of VSV G in the midgut enterocytes of ACA (n = 68) and ETH (n = 80) treated flies in the shaded areas. Data shown represents combined data from 3 independent replicates.

Figure S5.

Distribution patterns of YFP-tagged Rab GTPases in *Drosophila* midgut enterocytes and salivary gland cells. Fly lines (Zhang et. al., 2007;. DOI: 10.1534/genetics.106.066761Genetics 176:1307-22) inducibly and ubiquitously expressing each of 30 UAS-YFP-Rab GTPases for 3 days using the *da-GAL4, tub-GAL80^{ts}* driver were immunostained with chicken anti-GFP primary antibody and Alexa Fluor 488 goat anti-chicken secondary antibody (green). Actin (red) was labelled with Alexa Fluor 555 phalloidin, nuclei (blue) were stained with DAPI, and Discs large (magenta) was stained with mouse anti-Discs large primary antibody and Alexa Fluor 647 donkey anti-mouse secondary antibody. Scale bars represent 5 μm.

Figure S6.

Relative levels of VSV G^{WT} and VSV $G^{\Delta Y}$ in *Drosophila* midgut enterocytes. Permeabilized midgut tissues were used to determine whether the ΔY substitutions affect steady state levels of VSV $G^{\Delta Y}$ compared to VSV G^{WT} in the entire cell. The total levels of VSV $G^{\Delta Y}$ in enterocytes were significantly lower (18.5 times) than that of VSV G^{WT} (Pairwise Wilcoxon rank sum test: $p < 2.0 \times 10^{-16}$). VSV G expression was induced for 3 days under the *da-GAL4, tub-GAL80^{ts}* driver. VSV G was labelled with mouse anti-VSV G primary antibody and Alexa^{647}-conjugated donkey anti-mouse secondary antibody. Signal levels were measured using ImageJ (as described in Materials and Methods). Differences in the relative levels of VSV G (WT vs ΔY) could result from differences in translation efficiency, processing, protein half-life or turnover, and/or from variations between different fly lines. We therefore focused on the relative distribution patterns of the VSV G^{WT} and VSV $G^{\Delta Y}$ proteins in these studies.

Table S1.

Recipe of artificial *Drosophila* diet used in this study.

Figure 1

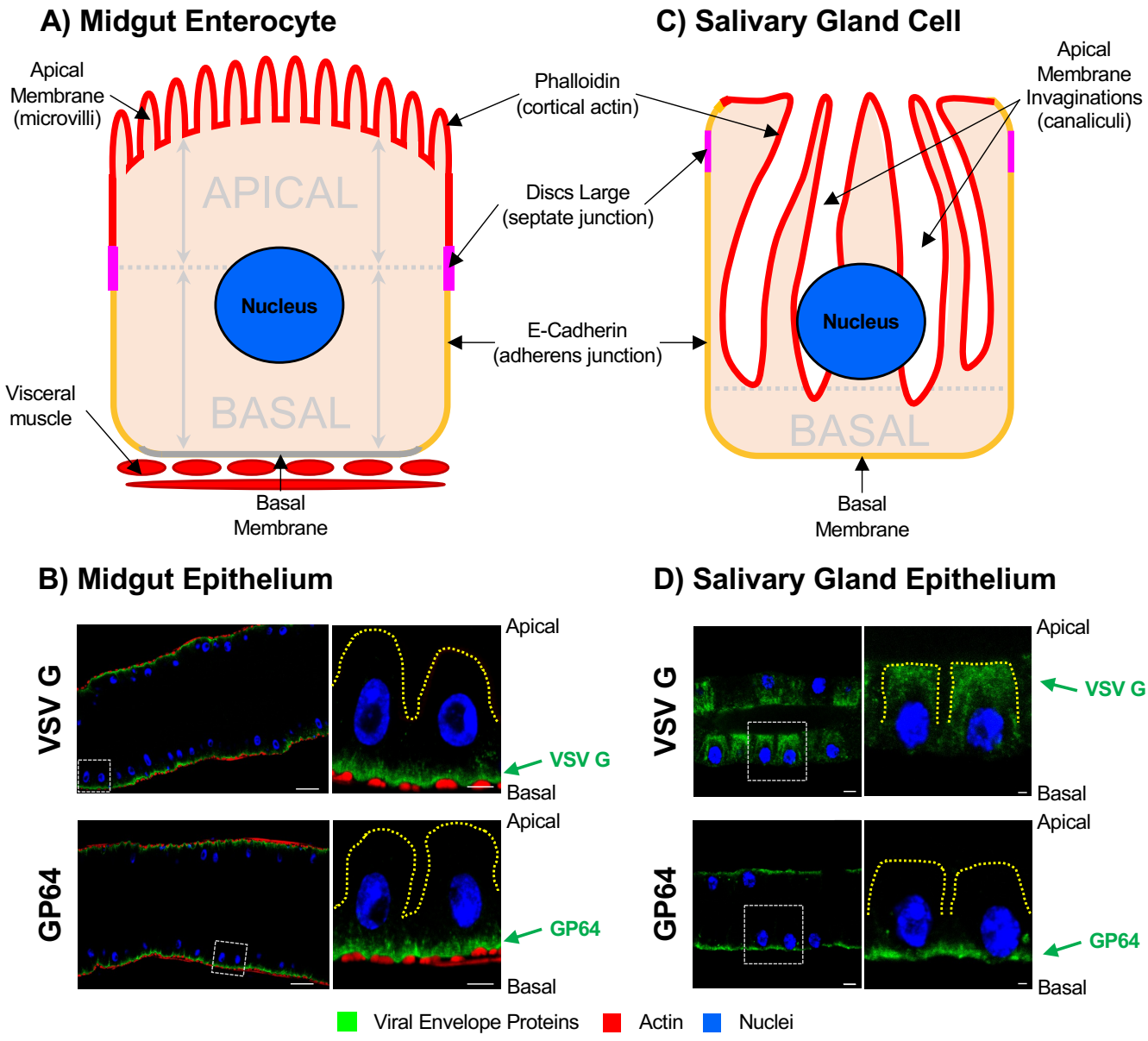
A) Midgut Enterocyte
Apical Membrane (microvilli)
APICAL
Nucleus
BASAL
Visceral muscle
Basal Membrane
Phalloidin (cortical actin)
Discs Large (septate junction)
E-Cadherin (adherens junction)
C) Salivary Gland Cell
Apical Membrane Invaginations (canaliculi)
Nucleus
BASAL
Basal Membrane
B) Midgut Epithelium
VSV G
Apical
VSV G
Basal
GP64
Apical
GP64
Basal
D) Salivary Gland Epithelium
VSV G
Apical
VSV G
Basal
GP64
Apical
GP64
Basal
Viral Envelope Proteins
Actin
Nuclei

Figure 2

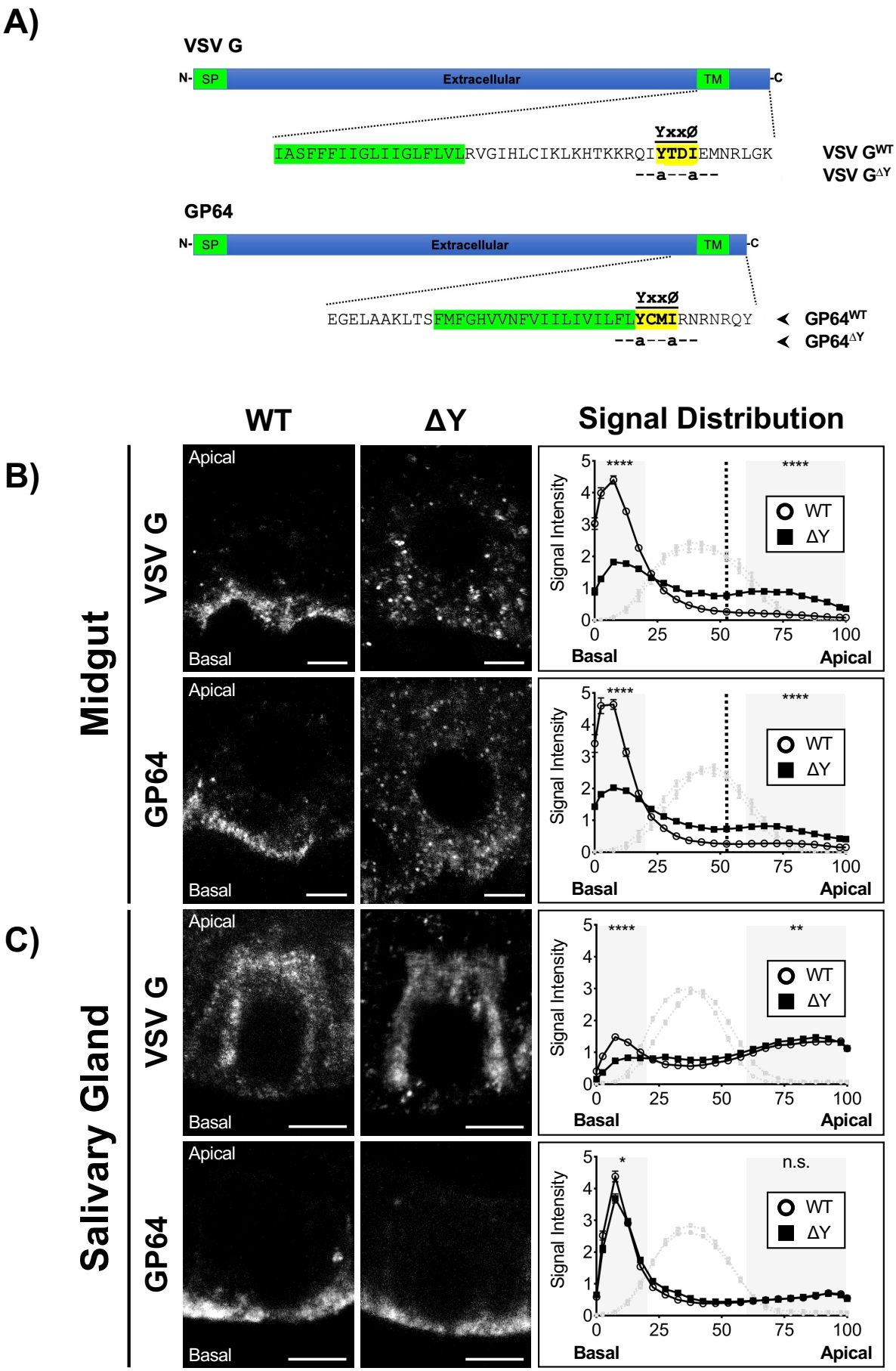
A)
VSV G
N-
SP
Extracellular
TM
-C
YxxØ
IASFFFIIGLIIGLFLVLRVGIHLCIKLKHTKKRQIYTDIEMNRLGK
--a--a--
VSV G^WT
VSV G^ΔY
GP64
N-
SP
Extracellular
TM
-C
YxxØ
EGELAAKLTSFMFGHVVNFVIILIVILFLYCMIRNRNRQY
--a--a--
GP64^WT
GP64^ΔY
WT
ΔY
Signal Distribution
B)
Midgut
VSV G
GP64
Apical
Basal
Signal Intensity
WT
ΔY
****
****
Basal
Apical
C)
Salivary Gland
VSV G
GP64
**
*
n.s.

Figure 3

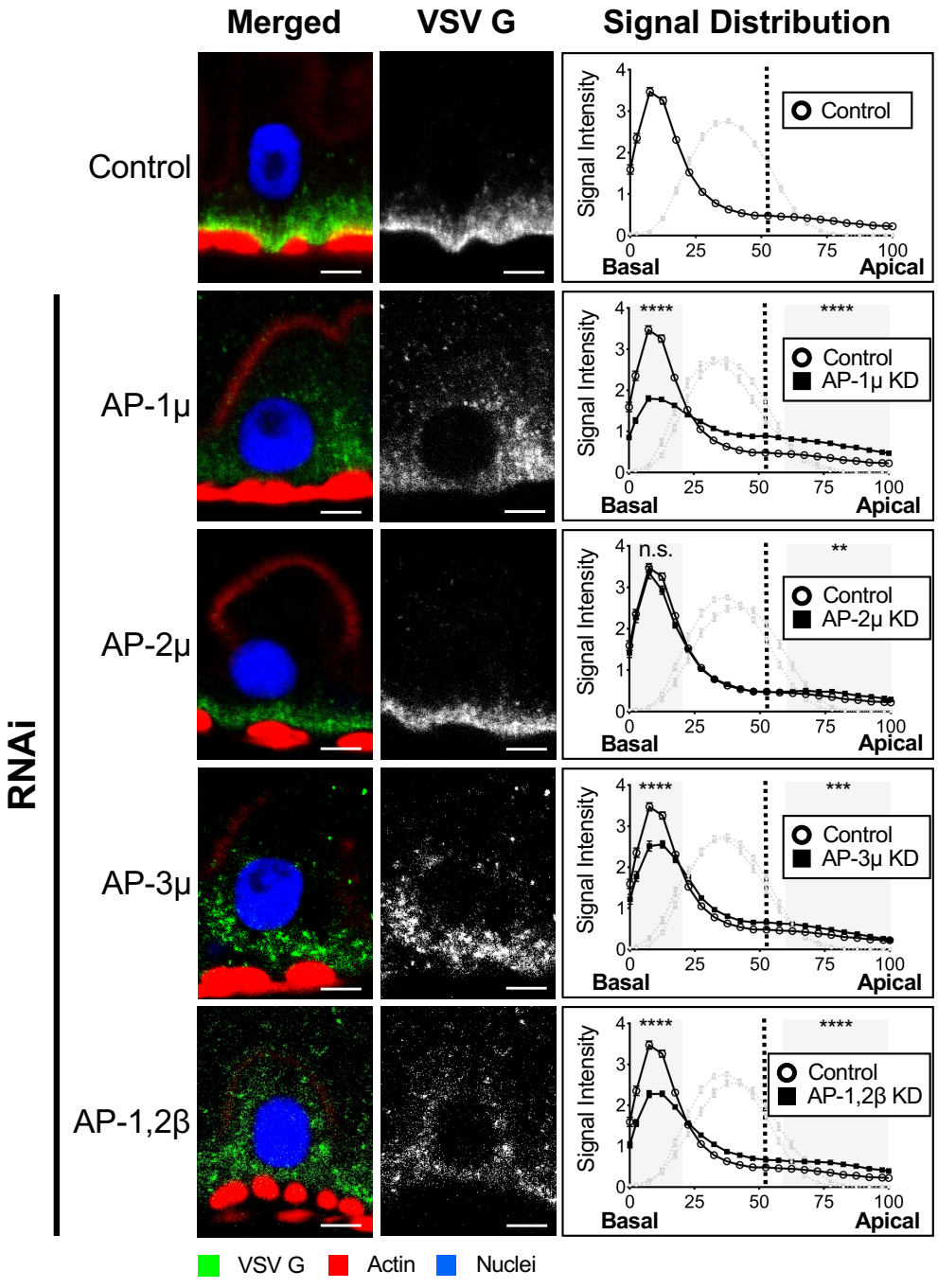
Merged
VSV G
Signal Distribution
Control
AP-1μ
AP-2μ
AP-3μ
AP-1,2β
RNAi
Signal Intensity
Basal
Apical
Control
AP-1μ KD
AP-2μ KD
AP-3μ KD
AP-1,2β KD
n.s.
**
***
****
VSV G
Actin
Nuclei

Figure 4

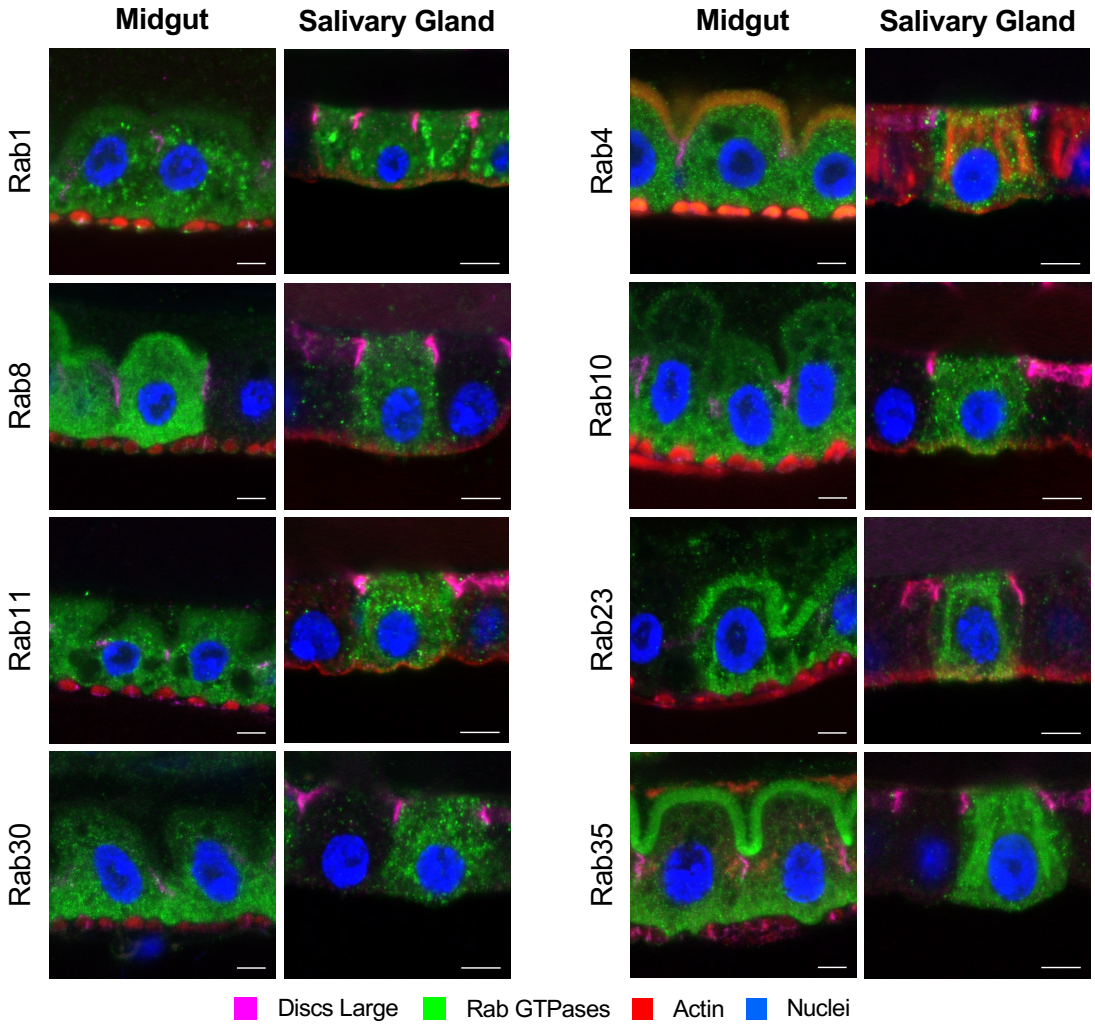
Midgut
Salivary Gland
Midgut
Salivary Gland
Rab1
Rab4
Rab8
Rab10
Rab11
Rab23
Rab30
Rab35
Discs Large
Rab GTPases
Actin
Nuclei

Figure 5

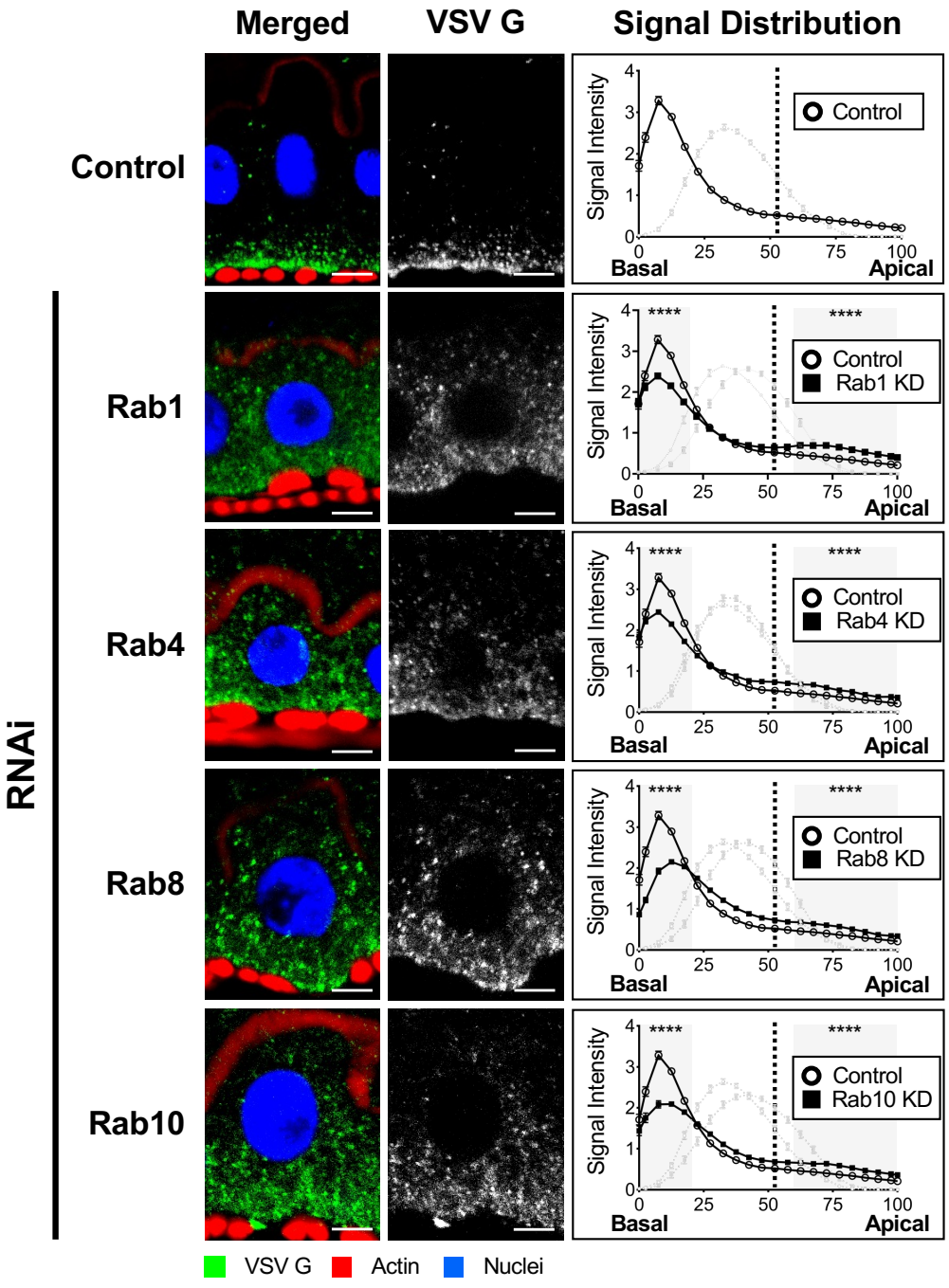
Merged
VSV G
Signal Distribution
Control
Rab1
Rab4
Rab8
Rab10
RNAi
Signal Intensity
Basal
Apical
Control
Rab1 KD
Rab4 KD
Rab8 KD
Rab10 KD
****
VSV G
Actin
Nuclei

Figure 5 (continued)

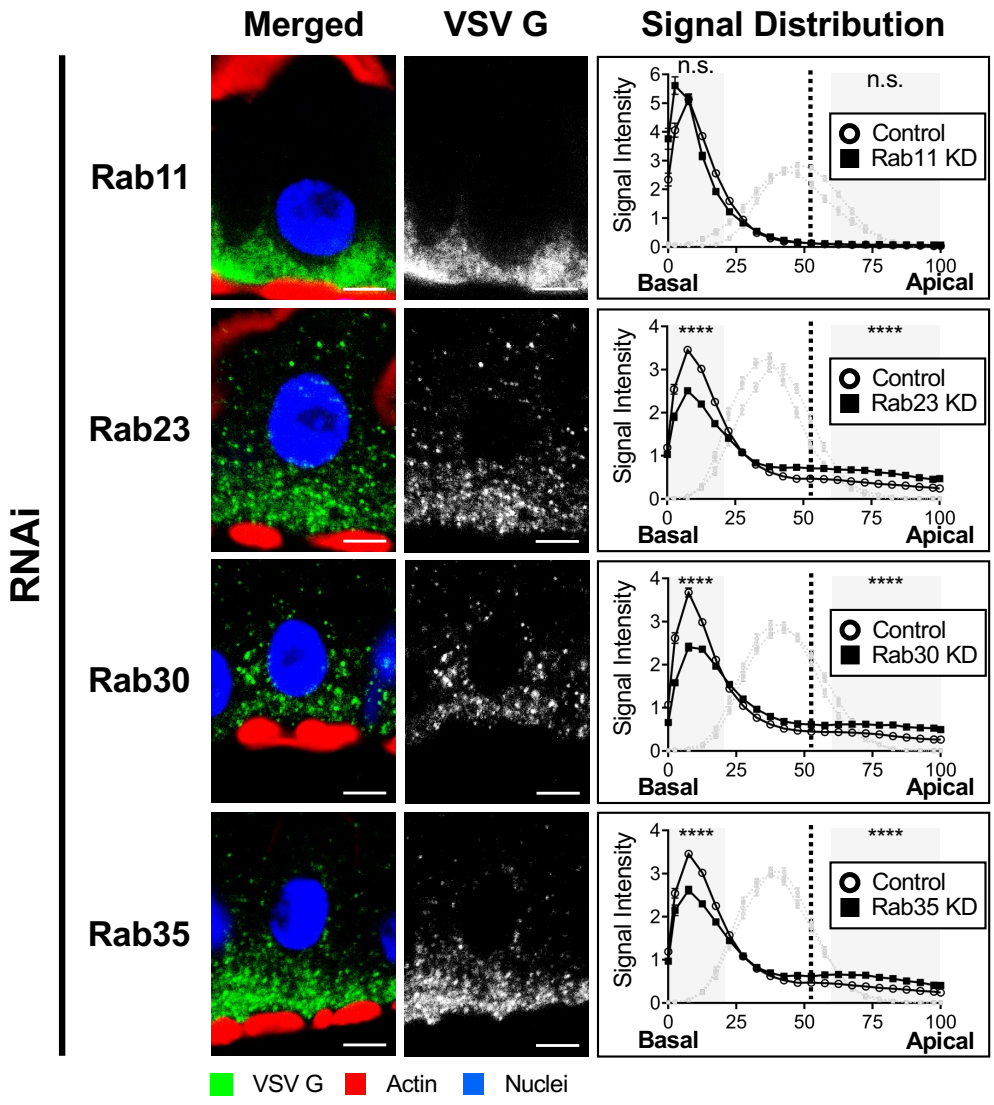

Supplemental Figures

Figure S1

A) Selection of regions of interest (ROI)

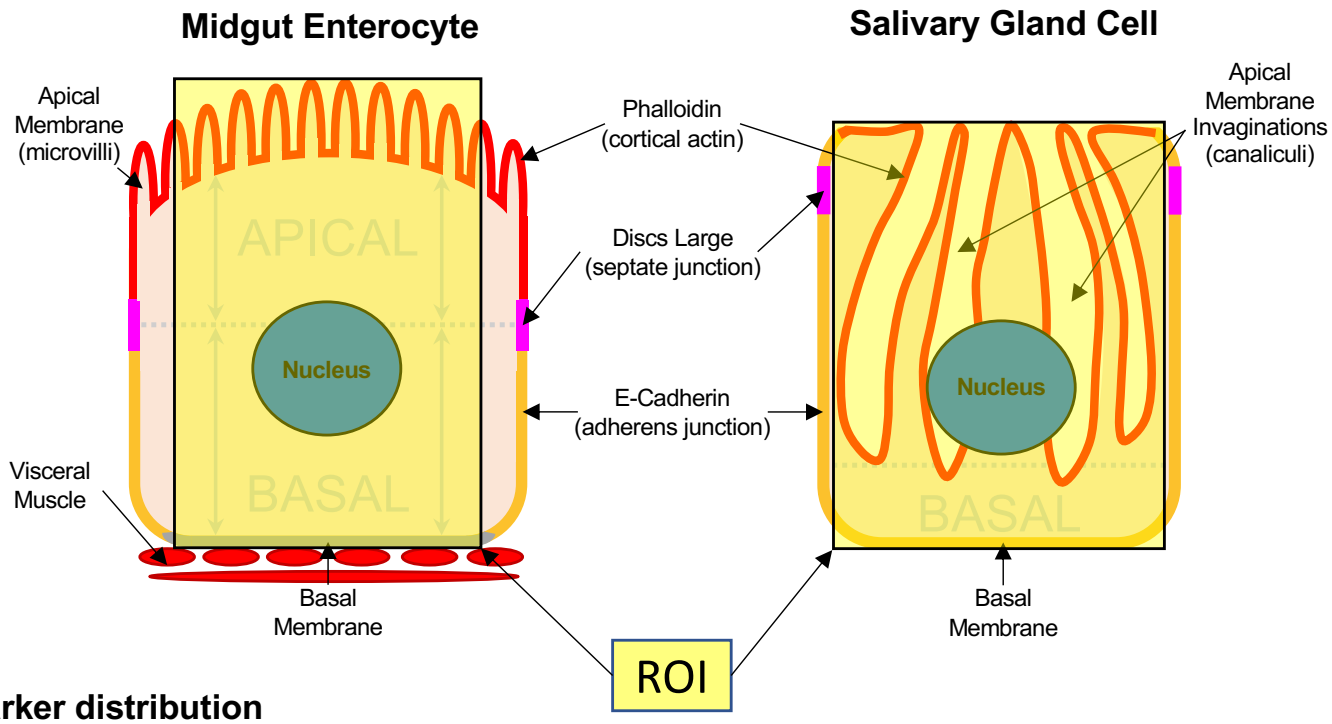

B) Marker distribution

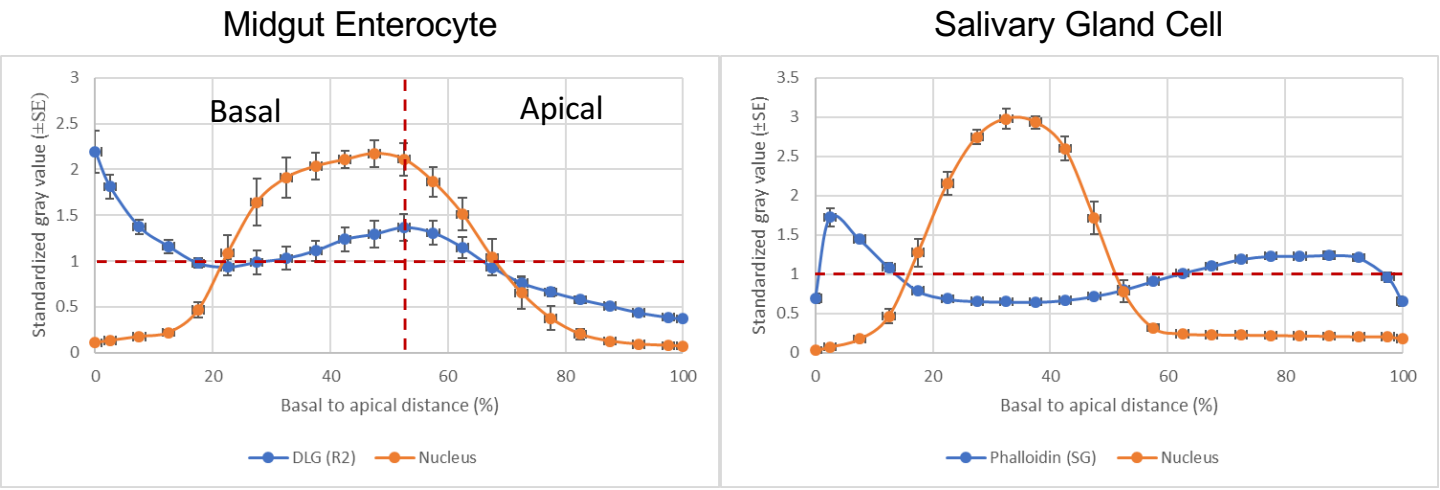

C) Regions used for statistical analysis

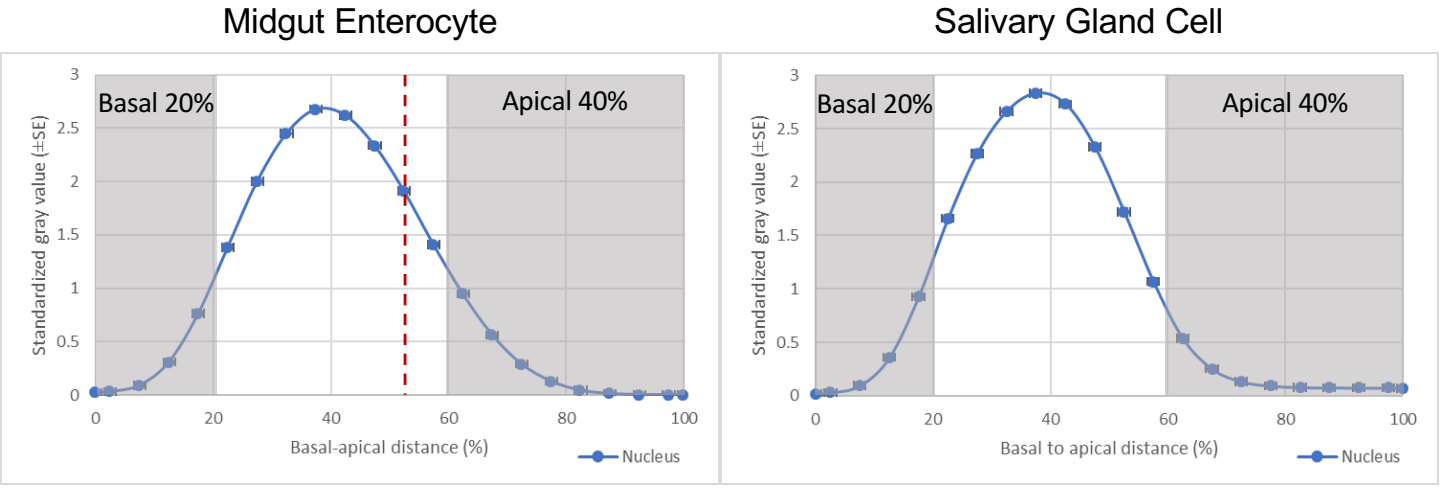

Figure S2A

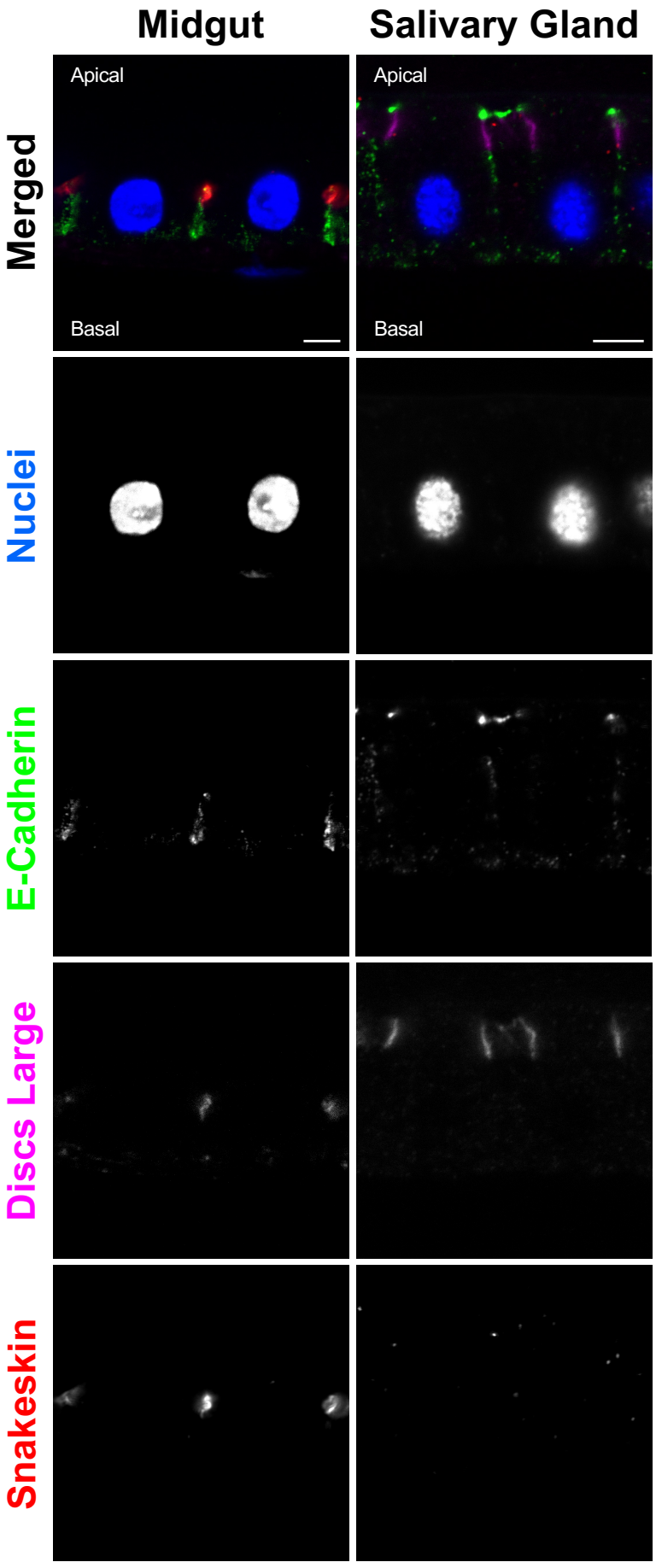
Midgut
Salivary Gland
Merged
Nuclei
E-Cadherin
Discs Large
Snakeskin
Apical
Basal
Apical
Basal

Figure S2B

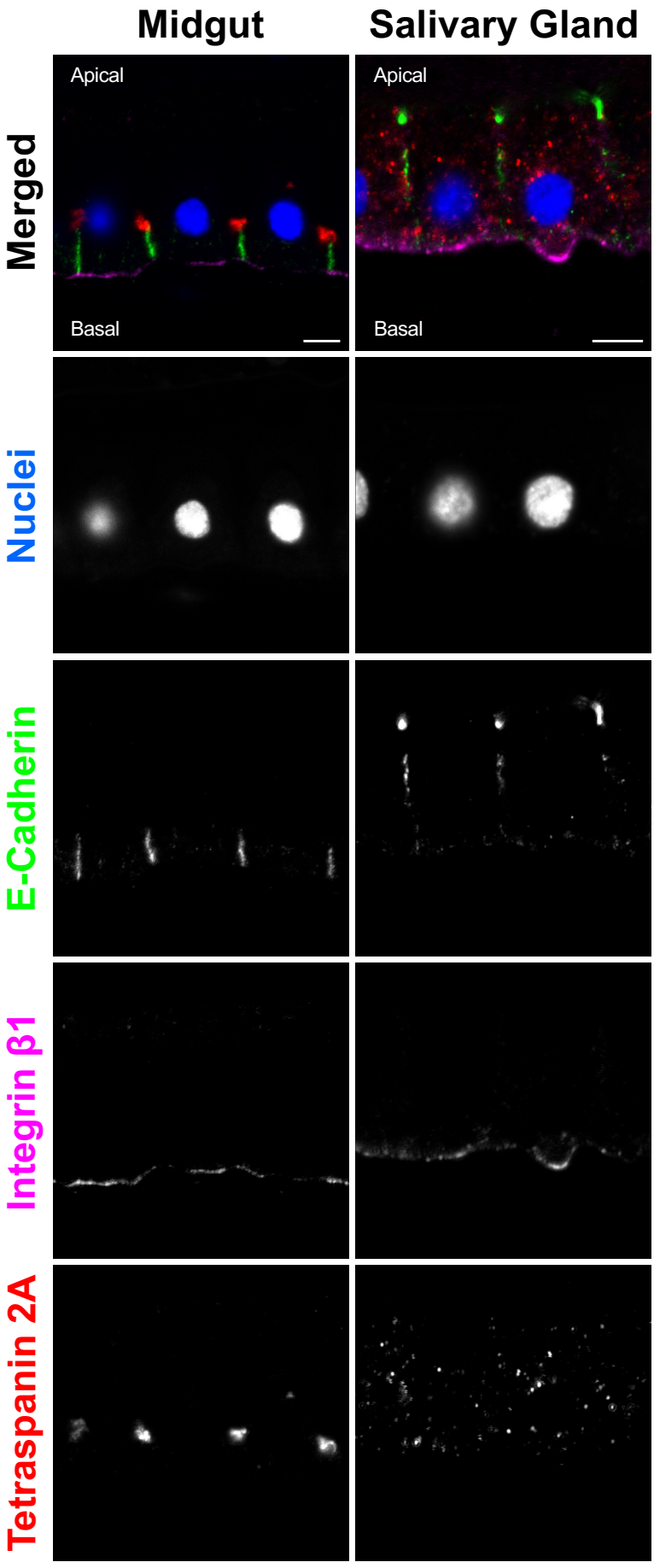
Midgut
Salivary Gland
Merged
Apical
Basal
Apical
Basal
Nuclei
E-Cadherin
Integrin β1
Tetraspanin 2A

Figure S2C

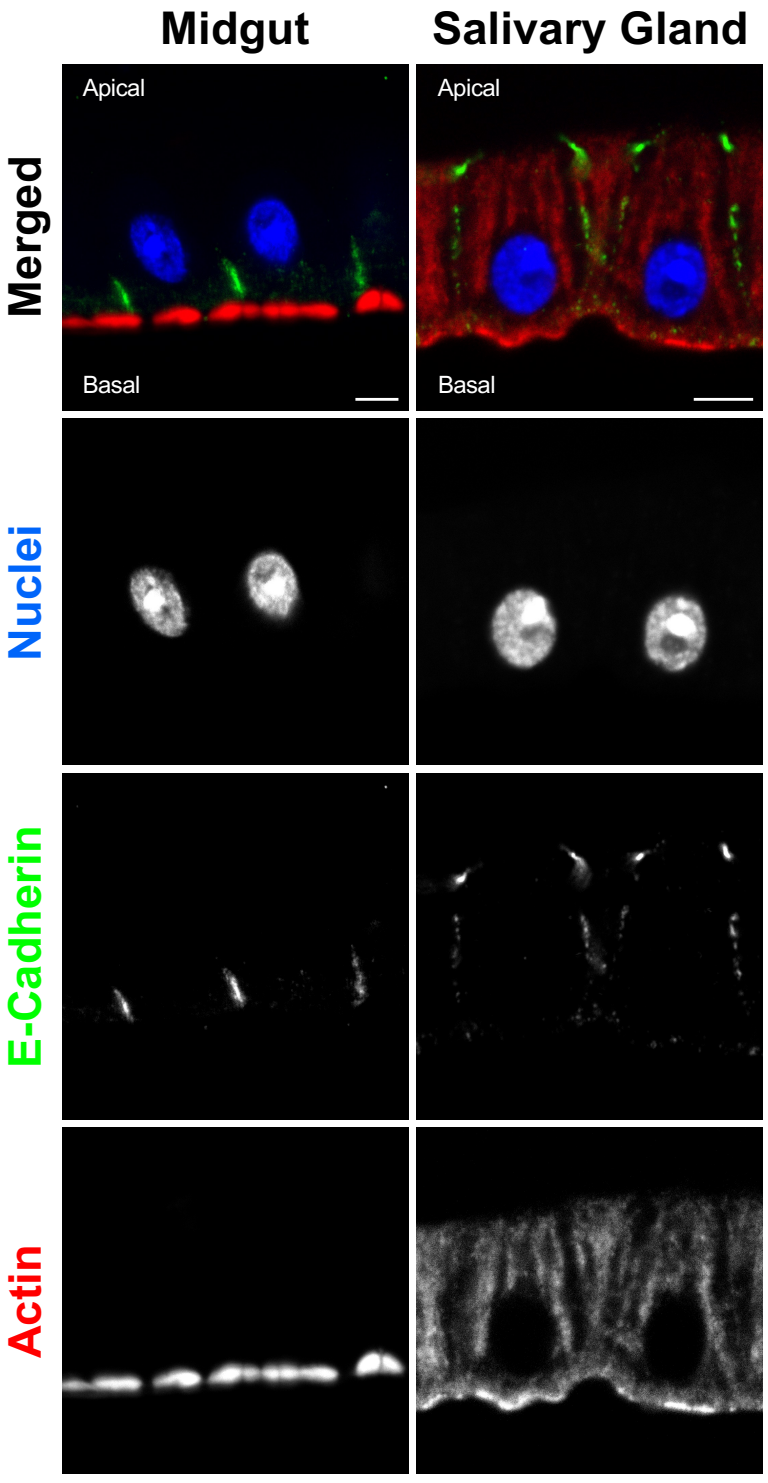
Midgut
Salivary Gland
Merged
Nuclei
E-Cadherin
Actin
Apical
Basal
Apical
Basal

Figure S3

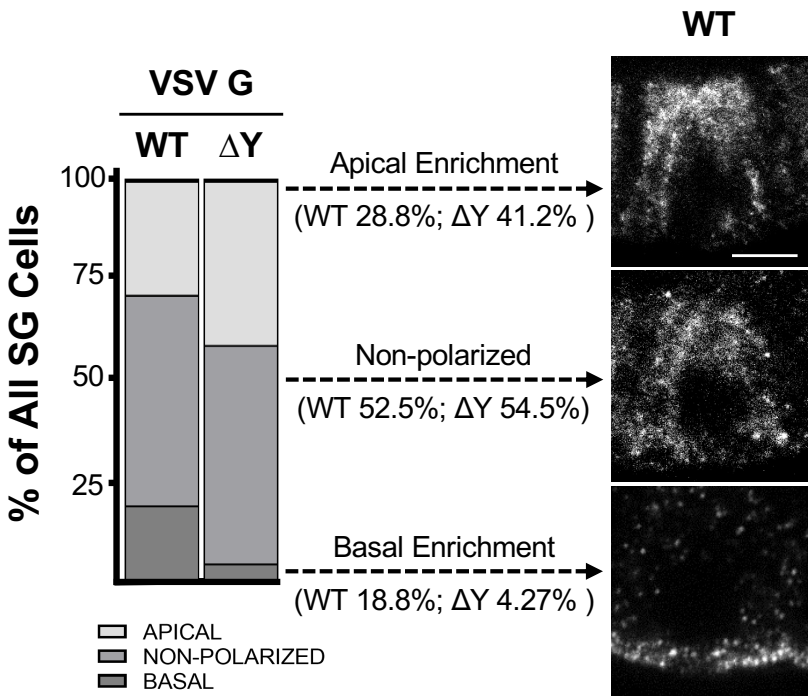
Distribution of VSV G in Salivary Gland Cells
WT
VSV G
WT
ΔY
100
75
50
25
% of All SG Cells
Apical Enrichment
(WT 28.8%; ΔY 41.2%)
Non-polarized
(WT 52.5%; ΔY 54.5%)
Basal Enrichment
(WT 18.8%; ΔY 4.27%)
APICAL
NON-POLARIZED
BASAL

Figure S4

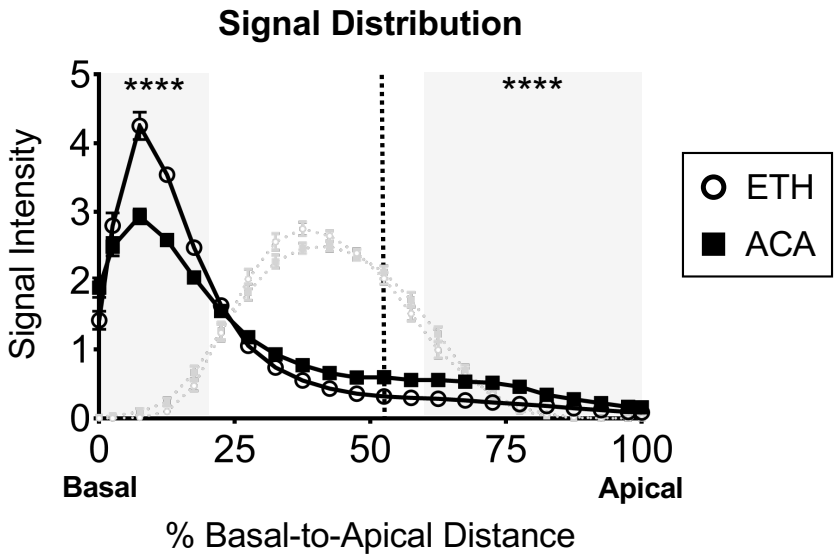
Signal Distribution
****
****
Signal Intensity
5
4
3
2
1
0
0
25
50
75
100
Basal
Apical
% Basal-to-Apical Distance
ETH
ACA

Figure S5A

Distribution patterns of YFP-Rab GTPases in midgut enterocytes and salivary gland cells

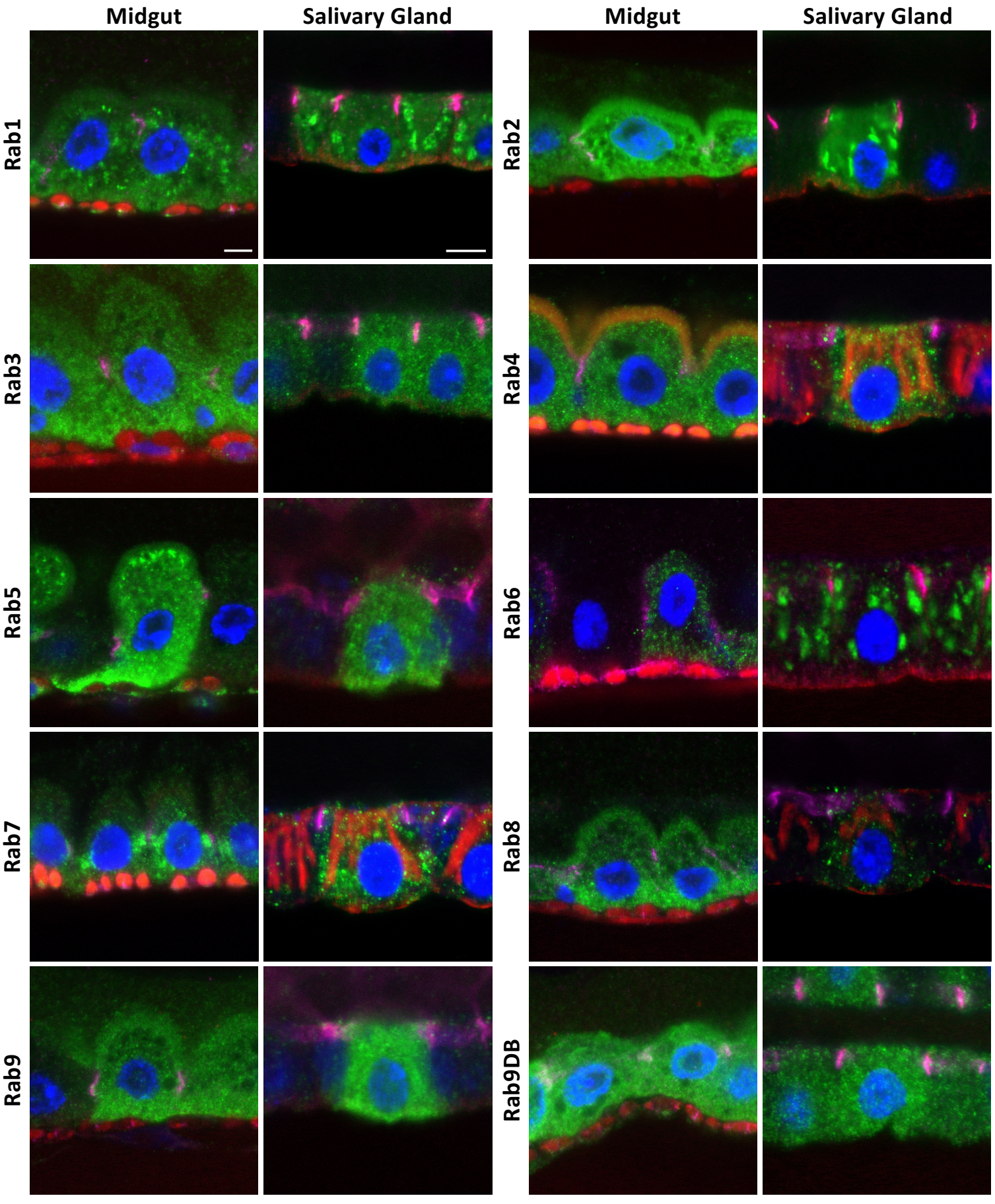

Figure S5B

Distribution patterns of YFP-Rab GTPases in midgut enterocytes and salivary gland cells

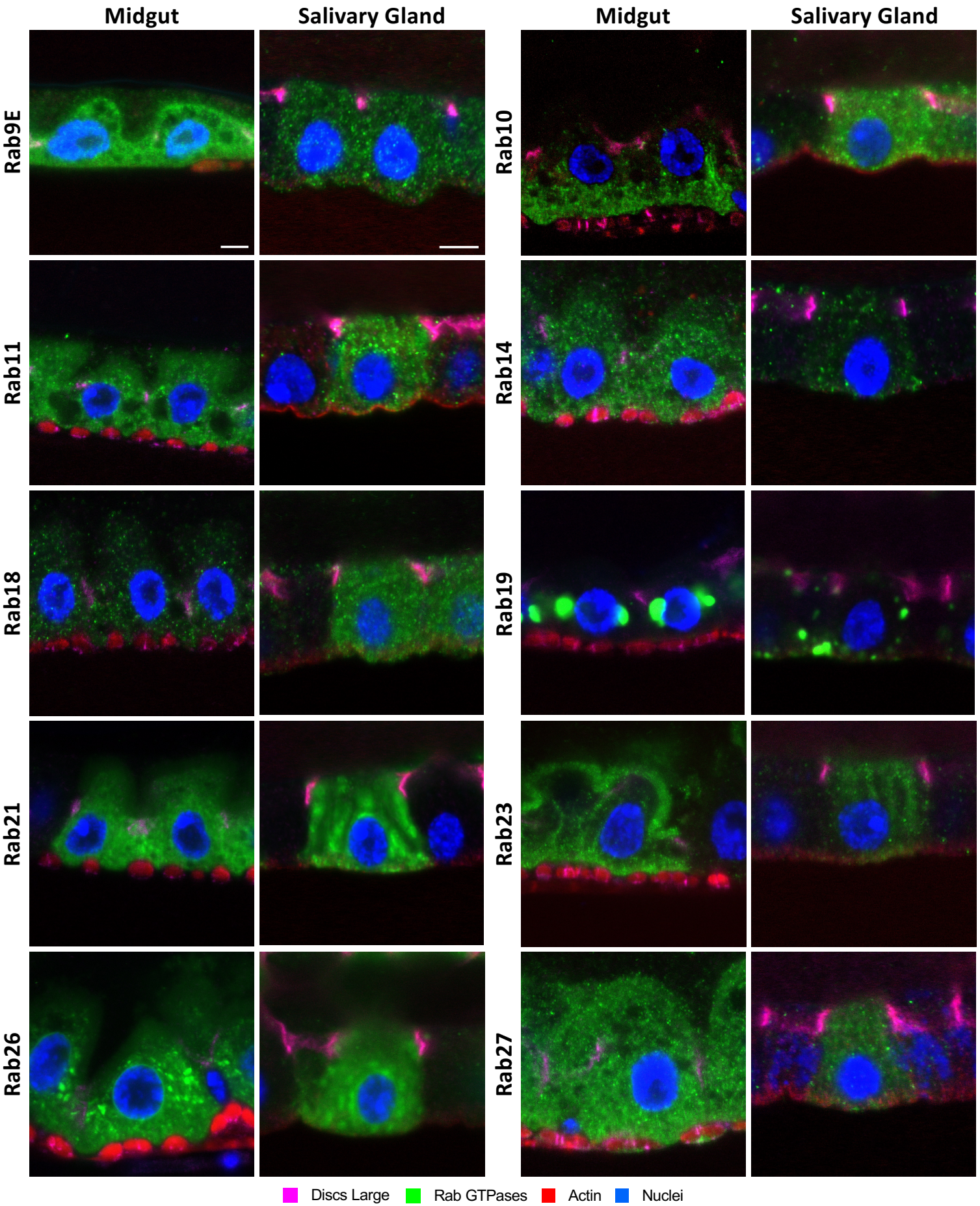

Figure S5C

Distribution patterns of YFP-Rab GTPases in midgut enterocytes and salivary gland cells

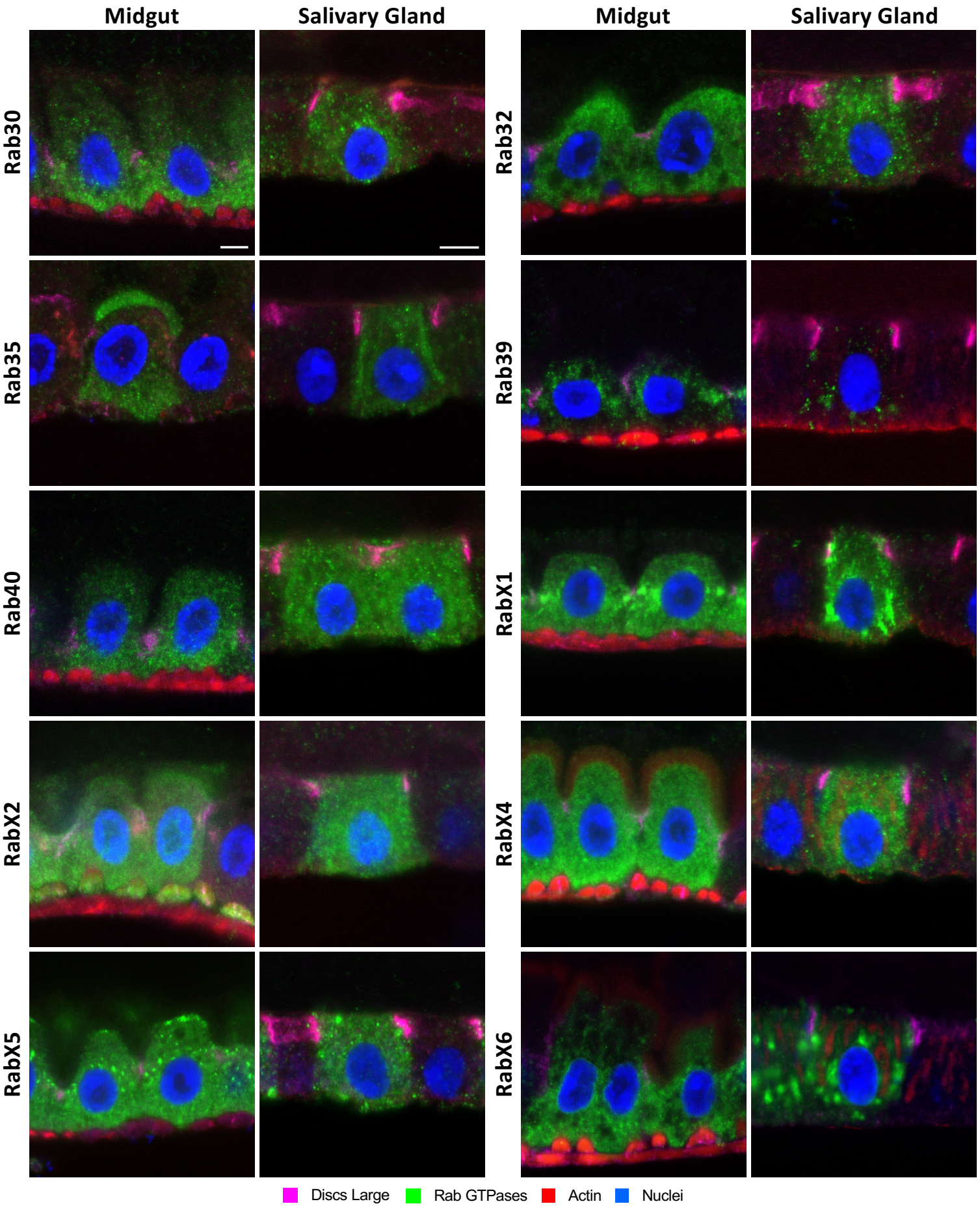

Figure S6

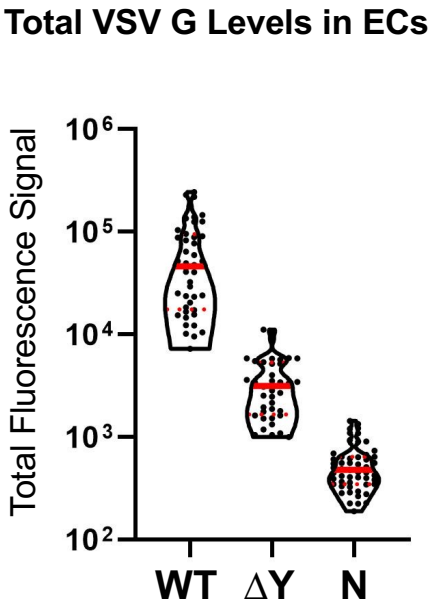
Total VSV G Levels in ECs
Total Fluorescence Signal
10^6
10^5
10^4
10^3
10^2
WT
ΔY
N

Table S1

Artificial Fly Food Recipe (1L)

Ingredient	Amount
Yeast	50g
Yellow Cornmeal	60g
Sucrose	40g
Agar	7g
Moldex (10%)	26.5mL
Acid Mix	12mL
Water	804.5mL

10% Moldex Recipe (1L)

Ingredient	Amount
Moldex	100g
Ethanol (95%)	1L

Acid Mix Recipe (500mL)

Ingredient	Amount
Water	270mL
Propionic acid	209mL
Phosphoric acid	21mL